The Design and Feasibility of a 10 mN Chemical Space Propulsion Thruster

by

Alexander Robert Bruccoleri

Submitted to the Department of Aeronautics and Astronautics
in partial fulfillment of the requirements for the degree of

Masters of Science in Aeronautics and Astronautics

at the

MASSACHUSETTS INSTITUTE OF TECHNOLOGY

June 2009

Author .....
Department of Aeronautics and Astronautics
May 18, 2009

Certified by .....
Paulo Lozano
Assistant Professor
Thesis Supervisor

Accepted by .....
David L. Darmofal
Associate Department Head
Chair, Committee on Graduate Students

The Design and Feasibility of a 10 mN Chemical Space Propulsion Thruster

by

Alexander Robert Bruccoleri

Submitted to the Department of Aeronautics and Astronautics
on May 18, 2009, in partial fulfillment of the
requirements for the degree of
Masters of Science in Aeronautics and Astronautics

Abstract

This thesis discusses the design of a ten milli Newton chemical propulsion system for providing approximately 200 m/s delta velocity to a five kg satellite. The nozzle is the focus of the experimental work, which involves building and testing ten 20x upscale 2D nozzles. The ten nozzles involve three classes, an ideal contour for 2D expansion, a 15 degree cone, and the ideal contour widened for the displacement thickness, each cut to 25%, 50% and 100% axial lengths. The last nozzle is a 100% axial length, ideal contour class, that is twice the thickness to see the effect of end wall boundary layer growth. The nozzles are tested in the MIT Space Propulsions Lab's vacuum chamber at sub atmospheric chamber pressures to match the throat Reynolds number with the micro nozzles. For the purposes of this specific design the Reynolds number is on the order of a 1,000; however, tests are done over a range of 200-1,400 to provide additional data to the community. The nozzle's coefficient of thrust efficiency is approximately 80% for Reynolds numbers greater than a 1,000 and the data suggest the efficiency drops below 50% at 200. The error becomes significant at low Reynolds number due to pressure measurement error, which reduces the quality of the results. The entire system is compared to the state-of-the-art in milli Newton class space propulsion systems and recommendations are given for propellant choice, valve and pump designs, and thermal management. For small delta velocity missions (≈ 200 m/s), a monopropellant chemical propulsion system is advantageous to current electric propulsion and cold gas thrusters due to the low system mass.

Thesis Supervisor: Paulo Lozano
Title: Assistant Professor

Acknowledgments

I would like to thank the United States Air Force Office of Sponsored Research for initiating this project (contract # FA9550-08-c-0007) and sponsoring an STTR between MIT and Ventions LLC. Dr. Jerry Guenette was my initial mentor from the MIT Gas Turbine Lab. Dr. Guenette was involved with previous micro rocket projects at MIT and his mentorship guided me from the initial concept towards running experiments. Dr. Adam London of Ventions was one of the founders of MEMS based rocket propulsion technology and I was fortunate to have his advice for nozzles and valves.

Many thanks goes to Professor Paulo Lozano of the MIT Space propulsion lab. Professor Lozano mentored me for the last two thirds of the project and provided laboratory and financial support for the project. Professor Martinez-Sanchez of the space propulsion lab also gave me valuable technical advice throughout the research. Randy Leiter of Busek Corporation also provided much help with refurbishing a thrust stand for the lab that was used extensively in this project. Todd Billings of the MIT Aero-Astro machine shop was very helpful in the use of the waterjet for cutting out nozzles and in teaching me how to weld plexiglass. And I would like to thank the MIT Gas Turbine Lab and the Space Propulsion Lab in general for support, office space and general research advice throughout this project. I listened to the course 16.120 and wrote a short Matlab program analyzing friction and heat transfer of nozzles as a volunteer for a group. I used that code in this thesis and I would like to thank group members Benjamin Glass, David Hall, Hiten Mulchandani, Rane Nolan and Shinji Tanaka for discussing the concepts and code with me.

I would like to give special thanks to the Department of Defense, National Defense Science and Engineering Graduate (NDSEG) Fellowship team for sponsoring me to complete this masters thesis. Without their support, this would not have been possible. Lastly I would like to thank my parents Dr. Robert Bruccoleri and Gloria Bruccoleri for their support throughout this work, and special thanks to my dad for helping me with LaTeX so I could write this manuscript.

Contents

List of Figures

List of Tables

Chapter 1

Introduction

In the past decades technology for Microelectromechanical systems (MEMS) has expanded greatly enabling orders of magnitude reductions in the size of aerospace hardware. Specifically in the last few years there has been an increasing interest in small (≈10 kg) satellites for reconnaissance, remote sensing, communications an education. As a result the need for a propulsion system has arisen to provide both primary and secondary propulsion maneuvers for such satellites. This thesis involves designing and analyzing the feasibility of a micro space propulsion system. This project was initiated as an Small Business Technology Transfer (STTR) between Ventions LLC and the MIT Gas Turbine Lab (GTL), and funded by the Air Force Office of Scientific Research (AFOSR). This thesis seeks to expand on the specific goals of that project to answer more general questions and provide useful data to future scientists and engineers.

1.1 Background of Space Propulsion Limitations

At present there is only one paradigm for providing propulsive force in space; expelling momentum out the spacecraft, also known as rocket propulsion. Other concepts have been proposed such as rotating tethers in the earths magnetic field [18], devices utilizing photon pressure [40] and a host of others that take advantage of the nearby earth or ambient environment [12]. Many of these concepts have merit and are under

development; however, only rocket propulsion has been developed and there are two main classes of rocket propulsion, chemical and electric propulsion. Chemical rockets convert thermal energy of a gas into kinetic energy, via expansion through a nozzle. Electric rockets use combinations of electric and magnetic fields to accelerate charged particles away from the spacecraft [27]. The momentum force generated by a rocket is;

$$F = \frac{dP}{dt}, \tag{1.1}$$

where P is the momentum of the expelled propellant. This is equal to the mass flow rate of propellant ($\dot{m}$) times the exhaust speed (u_e). Historically Aerospace engineers have divided the exhaust velocity by the gravitational acceleration (9.81 m/s^2) to give a value called specific impulse (I_{SP}) measured in seconds. This value represents the number of seconds one kilogram of propellant can produce $\approx$ 10 newtons of thrust. Formally,

$$I = \int F dt, \tag{1.2}$$

where I is the total impulse and F is the force, which leads to;

$$I_{sp} = \frac{I}{g_0 \int \dot{m} dt}, \tag{1.3}$$

which has the units of seconds. It is a matter of choice what one decides to use and I_{SP} will be used for this thesis; however, it is for all practical purposes the exhaust velocity, divided by a constant. For a given I_{SP} and assuming no other forces acting on the rocket, one can calculate the change in a rocket's velocity knowing the initial and final mass m_i & m_f,

$$\Delta V = (I_{SP})\, g_0 ln(\frac{m_i}{m_f}). \tag{1.4}$$

This equation is quite powerful since it shows an exponential relationship between I_{SP} and initial and final mass. For sufficiently large ΔV missions or small I_{SP}s nearly all of the initial mass of the spacecraft will be propellant which is a clear limitation on the performance of the spacecraft. For chemical rockets the I_{SP} is limited to

about 500s; however, electric rockets are practically unlimited and can achieve I_{SP}s in excess of 5,000s. The key distinction is that chemical rockets utilize the chemical energy stored in the propellants, while electric rockets must use an external power supply since the propellant is energetically neutral. The power of an ideal rocket is,

$$Power = \frac{1}{2}\dot{m}u_e^2. \tag{1.5}$$

This means that for a given thrust, the power required increases linearly with I_{SP}. For all practical purposes the only power supplied available to spacecraft are solar panels or nuclear power generators. Both of which scale approximately linearly with power. This mass is one of the important limitations on I_{SP} for electric rockets and for missions of low velocity change, makes electric propulsion impractical unless a low mass power system can be implemented. Essentially there are two types of missions where chemical propulsion is viable, high thrust and/or low ΔV missions.

1.2 Motivation for Micro Chemical Propulsion

The propulsion requirements for small satellites ranges from a few m/s ΔV to several km/s ΔV. For this project the ΔV requirement is given as 200 m/s from the Air Force over the lifetime of the mission. As a result the propulsion system has to provide both primary and secondary propulsion maneuvers. The difference between primary and secondary propulsion is arbitrary; however, primary propulsion refers to moving the satellite into a different orbit, whereas secondary propulsion is used to maintain a given orbit by countering orbital perturbations such as drag, solar pressure etc. For a micro satellite it is desirable to simplify the system by having one propulsion system for all the maneuvers and a thrust level of approximately 10 mN provides this. Maneuvers $\approx 10^2$m/s would take $\approx$ one day, and shorter maneuvers even less time. (Furthermore 10 mN was also a requirement of the Air Force.)

At present the state-of-the-art in milli Newton class chemical propulsion is a cold gas Butane propulsion system, with an I_{SP} of 70s [35]. This propulsion system is

unique since the Butane is stored as a liquid and it expands as a gas enabling high density storage capability. Alternatively for electric propulsion, the Busek BHT-200 is a state-of-the-art electric thruster and it produces 12.8 mN of thrust with an I_{SP} of 1,400s [35]. The thruster itself weighs several kgs and it requires 200 kW to operate. The thruster's mass alone makes it unsuitable for low ΔV missions. Therefore a low mass propulsion system with a higher I_{SP} than cold gas is desirable for micro satellite propulsion.

1.3 Motivation for Micro Nozzle

Cold Gas propulsion is the simplest form of rocket propulsion. Essentially a gas at high pressure and ambient spacecraft temperature is expanded through a nozzle to the vacuum of space creating a high velocity jet. One can think of the expansion process through the nozzle as an exchange of thermal to kinetic energy. Assuming enthalpy is conserved and a calorically perfect gas,

$$c_P T_s + \frac{1}{2}u^2 = c_P T_T, \tag{1.6}$$

where c_P is the heat capacity at constant pressure, T_s is the static temperature, u is the flow velocity and T_T is the total or stagnation temperature. Rearranging terms yields the following expression for exhaust velocity,

$$u_e = \sqrt{2c_P(T_0 - T_e)}. \tag{1.7}$$

This equation shows a square root relationship between rocket chamber temperature and exhaust velocity. As a result to improve the I_{SP} of a cold gas rocket by a factor of two, the temperature difference needs to be increased by a factor of four, which is well within range with either a monopropellant that decomposes exothermically or a reaction of two propellants. Another alternative is to use solid fuels; however, that presents a problem for restarting the thruster and is not considered for this project [8].

A liquid propulsion system in its simplest form consists of a chemical reaction chamber, nozzle, propellant tanks, a pressurizing system such as a high pressure tank or pump, valves and plumbing to connect the system together and a power supply to operate the valves to control the system. All of the components are interrelated and the analysis begins with the nozzle. It is assumed and later experimentally verified, that a throat Reynolds number of 1,000 or greater will suffice to prevent viscous losses from decreasing the isentropic nozzle efficiency below 80%. The Reynolds number is the ratio of a flows inertia forces to viscous forces and is defined,

$$Re = \frac{\rho U D}{\mu}, \tag{1.8}$$

where ρ is the density, U is the velocity, D is a characteristic length and μ is the dynamic viscosity. In the case of a rocket the velocity is the throat velocity, and the characteristic length is the throat diameter. For a given thrust, increasing the chamber pressure decreases the radius of the nozzle and increases the density.

$$T = \dot{m} u_e = \rho_1 Area_1 u_{e1}^2 = \rho_2 Area_2 u_{e2}^2 \tag{1.9}$$

Exhaust velocity is assumed the same and the ratio of throat conditions to exit conditions is also assumed the same. Furthermore, $Area(A) \propto D^2$, and $\rho \propto P$, which leads to;

$$P_1 D_1^2 = P_2 D_2^2, \frac{P_1}{P_2} = \frac{D_2^2}{D_1^2}. \tag{1.10}$$

This means as the pressure is increased the density goes up linearly and the nozzle radius goes down inversely as the square root of pressure. This means the $Re \propto \sqrt{Pressure}$ for constant thrust, and therefore high pressures and smaller sizes should be used to minimize the viscous losses in nozzles. It was decided by Ventions LLC and MIT that a chamber pressure of approximately 10 atm and a throat width of 35 μm would be a reasonable choice to achieve a Reynolds number of a 1,000. The design and feasibility of such a thruster is the focus of this thesis.

1.4 Motivation for Experimental Work

A space propulsion system ideally should propel the spacecraft to the desired velocity while taking up as little on board resources as possible. Mass, volume and power are the main resources a propulsion system requires and the micro chemical rocket should minimize its use of them. As will be discussed later, the valves, plumbing and nozzle are very small and their combined volume is on the order of cm^3. The main consideration for the propulsion system is fuel mass and tank volume. The propellant tanks should be held at 40 atm due to pressure losses in the fuel lines and reaction chamber to achieve a nozzle entrance pressure of 10 atm [16]. The most conservative system approach is to pressurize the propellant with a high pressure gas such as helium and utilize regulators and valves to control the flow. Two configurations are analyzed for system mass; a single tank containing both the propellant and the helium, the other, a propellant tank initially full of propellant and a separate pressurant tank.

The first configuration is the simplest; however, it requires the most volume and mass. High initial pressures are required since the as the gas expands it loses pressure. If the gas expands adiabatically, there is a simple relationship between initial and final pressure and volume,

$$PV^{\gamma} = constant, \tag{1.11}$$

where γ is the ratio of specific heat at constant pressure to the specific heat at constant volume. This means for a tank which initially is 40% fuel requires the initial pressure to be roughly 2.33 the final pressure. This is particularly problematic for a single tank since that pressure acts over a large area and requires a lot of structural material.

The two tank configuration is slightly more complicated but less massive and smaller. The tank pressure is held constant throughout the expansion process which occurs adiabatically. The pressurant volume can then be found using the first law of thermodynamics and the ideal gas law with the assumption of adiabatic walls,

$$V_{He} = \frac{(\gamma)P_{propellant}}{P_{He-initial} - P_{He-final}} V_{propellant} \tag{1.12}$$

In both cases the tanks are assumed thin walled and made from Titanium with a yield stress of 8.3x10^8 Pascals (Pa) [3]. The wall thickness tw can easily be found,

$$tw = \frac{Pr}{2\sigma}, \tag{1.13}$$

where P is the pressure, r is the tank radius, and σ is stress. With a safety factor of 3 the tank masses are calculated as a function of mission ΔV. The tank mass plus the fuel mass is the dominant mass of the propulsion system and this limits the range of missions where a chemical propulsion system is advantageous. The I_{SP} of the propulsion system is calculated from a chamber temperature of 1,000 K for Hydrogen Peroxide and 875 K for Hydrazine, with a nozzle pressure ratio of 226:1. The friction losses are assumed to be 20% via experiments described in this thesis. This leads to an I_{SP} of 127 s for Hydrogen Peroxide, 160 s for Hydrazine and one last I_{SP} of 70 s for the hypothetical scenario where the nozzle efficiency is sufficiently poor that the I_{SP} equaled that of cold gas, 70 s. Below is a plot of the results:

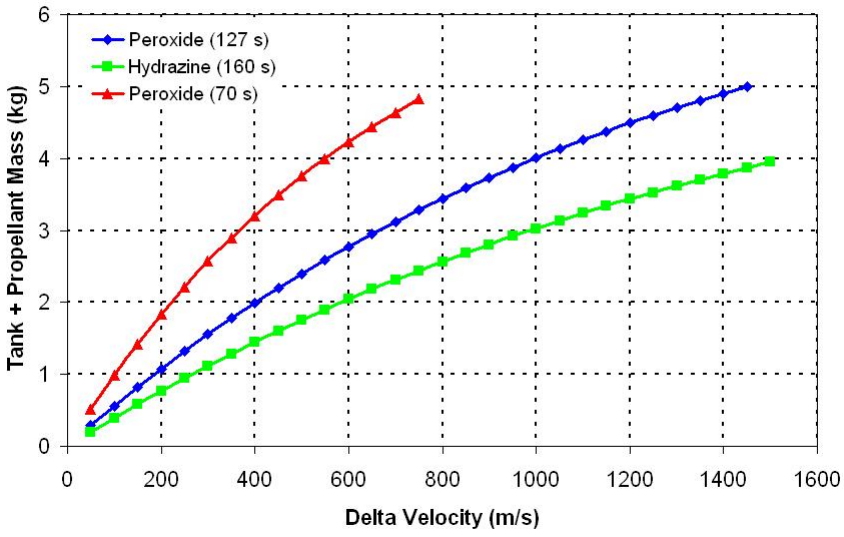

Figure 1-1: Propulsion system mass versus ΔV for a single configuration

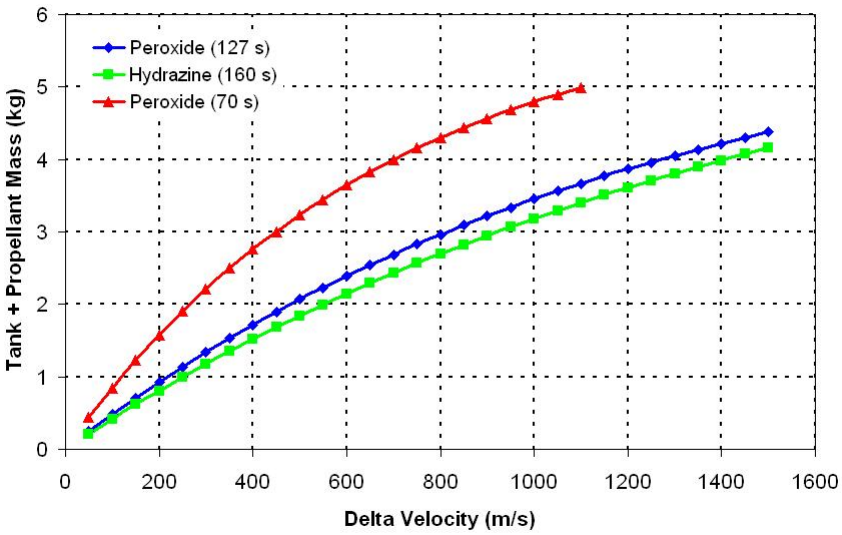

Figure 1-2: Propulsion system mass versus ΔV for a two tank configuration

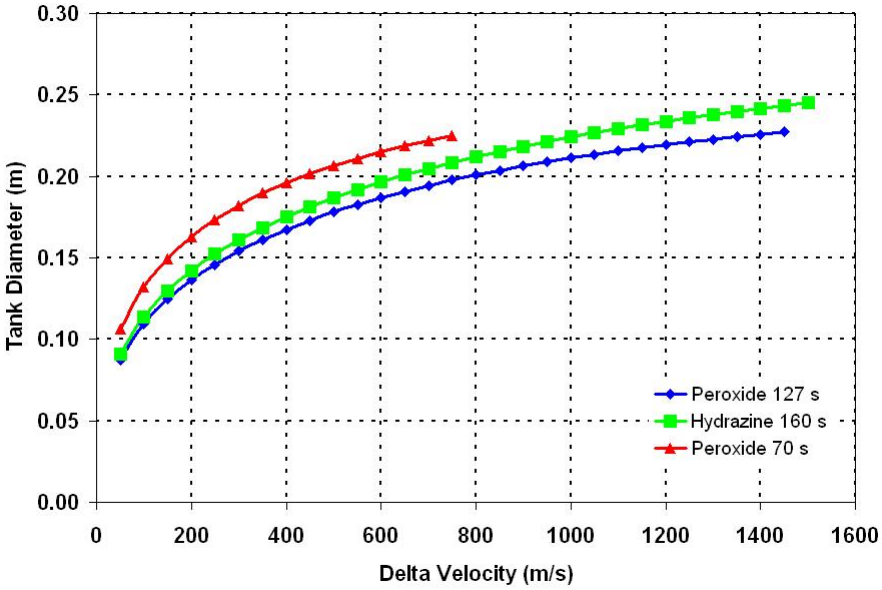

Figure 1-3: Propulsion system tank diameter versus ΔV for a single configuration

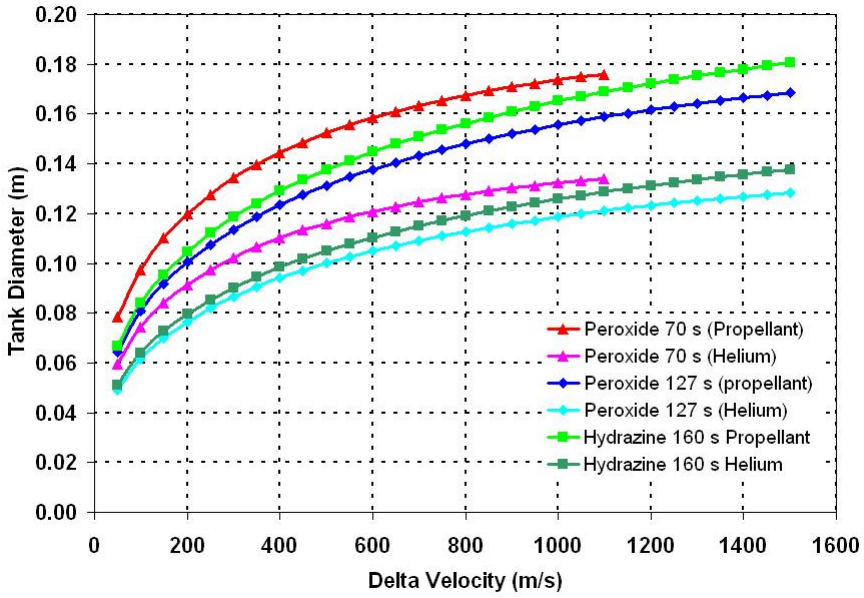

Figure 1-4: Propulsion system tank diameter versus ΔV for a two tank configuration

The ΔV possible where 20% of a 5 kg spacecraft is devoted to propulsion is approximately 200 m/s with the Hydrogen Peroxide or Hydrazine in either tank configuration. For Hydrogen Peroxide with an Isp of 70 s, the ΔV is roughly 100 m/s in both configurations. It is therefore very important that the nozzle efficiency be high (at least 80% of the isentropic efficiency) to substantially increase the spacecraft capability over a cold gas system. The main focus of the experimental work in this thesis is to demonstrate an efficient nozzle can be achieved at this scale.

It should be noted that the two tank configuration is less massive than the single tank; however, the difference is negligible for Hydrazine. Furthermore the single tank configuration is not held at constant pressure which means the thrust will vary as the tank losses pressure. The change in pressure is roughly a factor of 2 which might be acceptable for some missions. The plots are mainly for reference and to compare the two configurations. No designs are made to heat the helium with combustion gases to increase the internal energy and hence decrease the required helium. The tank diameters may also be of interests for some applications where space on a launch vehicle is the limiting factor as opposed to satellite mass. For a single tank configuration the diameters range from 12 to 16 cm and for the dual tank configuration, the

diameters range from 9 to 12 cm for the propellant and 7 to 9 cm for the Helium. All of these are quite large with respect to cubesats for example, which are limited to approximately 10 cm on a side and 1 kg of mass [8]. The satellites utilizing this type of propulsion will likely be larger then cubesats but still of the same order of magnitude and tradeoffs between volume and mass are likely decisions for future spacecraft engineers.

1.5 Past Micropropulsion Research

Low Reynolds number nozzle research started in the early 1970s with research by Massier et al. who tested nozzles at Reynolds numbers from approximately 600 to 10^6 [32]. They found the Coefficient of discharge (C_D) was greater then 94% for the lower Reynolds numbers and 98% for higher values. Where C_D is defined to be;

$$C_D \equiv \frac{\dot{m}}{\dot{m}_{1DIsentropic}} = \frac{1}{C}\frac{\dot{m}\sqrt{T_0}}{P_0 A_*}, \tag{1.14}$$

where T_0 and P_0 are the chamber temperature and pressure respectively,A_* is the throat area and C is a constant. A similar study was later done by Kuluva and Hosack, except the Reynolds numbers ranged from approximately 50 to 1000 [23]. The C_D ranged from .4 at the lower Reynolds numbers to .8 for higher values which demonstrated severe frictional losses at low Reynolds numbers. Both of these studies used conical nozzles and a more substantial study was done by Grisnik et al. [15]. They studied a conical nozzle, trumpet, bell and sharp face orifice at Reynolds numbers from 500 to 9000. They results were similar as the C_D ranged from about .8 to .95 over the range of Reynolds numbers tested. The sharp orifice remained relatively constant at .97 which demonstrates the significance of the frictional effects building up axially along the nozzles. Furthermore I_{sp} efficiencies were also measured and they ranged from 70-90% for the nozzles and 55-70% for the orifice. I_{sp} efficiency was calculated from the ratio of experimental I_{sp} (measured thrust divided by mass flow rate) to the theoretical maximum.

Independent of this nozzle research, investigations on micro rocket components became prevalent in the 1990s when manufacturing processes made submicron resolutions possible. The key design challenges were outlined by Mueller and Ketsdever in 1999 for both chemical and electric propulsion [22]. They outlined micronozzle scaling issues at low Reynolds flow and also looked at the basic continuum assumption in these flow regimes. They concluded that kinetic modeling via the Direct Simulation Monte Carlo (DSMC) [4] approach was useful for Reynolds numbers below 250. They also looked at combustion scaling issues on a small scale and determined the low residence time would yield large challenges for bi-propellants; however, monopropellants would be ideal due to the low mass flow rate. Furthermore they identified heat transfer and thermal management as issues for chemical propulsion. Their analysis of electric propulsion highlighted the issue of confinement scaling parameters. Specifically, large magnetic fields are required for traditional Hall and Ion thrusters to confine the plasma to prevent wall corrosion, which is a substantial technical challenge.

At about the same time a large effort was mounted by the MIT Microsystems Technology Laboratories (MTL) and the Gas Turbine Lab (GTL) to experiment with MEMS rocket propulsion technology. Two notable projects were completed by Bayt [37] and London [25]. Bayt's work was similar to this project in that he studied the effects of low Reynolds flow on nozzle efficiency. He studied nozzles with throat widths of 10-25 microns, with a 20 degree expansion ratio. He built a series of nozzles with expansions ratios ranging from 5.4:1 to 16.9:1 and throat Reynolds numbers ranging from approximately 200-4000. His results showed thrust efficiencies below 75% for Reynolds numbers below 1,000 in all tests. His work demonstrated the feasibility of fabricating micronozzles and produced substantial data for low Reynolds number flow.

In contrast to Bayt's work, London's experiments had two orders of magnitude higher thrust. Furthermore he designed a complete bi-propellant MEMS propulsion system on the order of 1 N of thrust. The motivation behind the project was to take advantage of the favorable scaling relations for thrust chambers at a small scale. The thrust of a rocket is proportional to the surface area (L^2); however, the mass

is proportional to the volume (L^3). As a result the thrust to weight goes up as the propulsion system becomes smaller. London built and tested a series of thrusters utilizing gaseous Oxygen and Methane propellant, and cooled with an external water coolant. Heat management ultimately limited the tests; however, the work demonstrated MEMS technology could be used to build rockets. Christopher Protz [36] did a similar project to London at MIT and experienced failures in the cooling passages due to manufacturing errors. Both projects aimed at producing fully regeneratively cooled bi-propellant microrockets with Peroxide and Kerosene. Liquid propellants are advantageous since they are much denser and reduce the tank mass and volume on a spacecraft.

Chapter 2

Micronozzle Analysis

2.1 Thrust Efficiency

There are several different types of efficiency that are considered for flow through a rocket nozzle. The first is the thermodynamic velocity efficiency which is the ratio of the thrust during a perfectly isentropic expansion to the thrust if the gas to expanded to zero pressure and temperature. A gas expanded to zero pressure and temperature has converted all the enthalpy in the fluid to thrust. For a rocket nozzle the velocity efficiency is

$$\eta_{isentropic} = \sqrt{\frac{T_{total} - T_{exit}}{T_{total}}}. \tag{2.1}$$

This is a theoretical maximum given the laws of thermodynamics; however, it represents an efficiency since not all of the enthalpy in the fluid can be converted to thrust for a non zero exit temperature. The other efficiency looks at the ratio of the thrust measured to the thrust achieved with a perfect isentropic expansion. A thrust coefficient (C_F) is defined,

$$C_{\mathcal{T}} \equiv \frac{\mathcal{T}}{P_0 A_t}, \tag{2.2}$$

where $\mathcal{T}$ is the thrust, P_0 is the chamber pressure and A_t is the throat area. This result is directly measured experimentally. The theoretical $C_{\mathcal{T}}$ is the combination of the thrust due to mass flow leaving the nozzle plus the contribution due to the

difference in pressure between the nozzle exit pressure and the ambient pressure;

$$C_{\mathcal{T}ideal} = \sqrt{\frac{2\gamma^2}{\gamma-1}\left(\frac{2}{\gamma+1}\right)^{\frac{(\gamma+1)}{(\gamma-1)}}\left[1-\left(\frac{P_e)}{P_0}\right)^{\frac{(\gamma-1)}{\gamma}}\right]} + \frac{P_e - P_a}{P_0}\frac{A_e}{A_t}, \tag{2.3}$$

where P_e is the exit pressure, P_a is the ambient pressure and A_e is the exit Area. For the purposes of this paper, the nozzle efficiency is the ratio of the measured $C_{\mathcal{T}}$ to the ideal $C_{\mathcal{T}ideal}$. The I_{sp} efficiency will be similar to the thrust efficiency and generally larger due to the effects of back pressure. A more complete description can be found in chapter 4.

2.2 Basic Modeling of Friction

A priori, a nozzle with a throat on the order of microns appears to suffer drastically from friction. In typical rockets with throat diameters on the order of 10 cm, the boundary layer is a few millimeters. In this study's nozzle, the maximum dimension of the nozzle is on the order of millimeters, which certainly casts doubt on the prospect of achieving high efficiency flow. This analysis quantifies the effect of friction to get a first order approximation. The Reynolds number as defined in chapter one is one measure of friction and it is the ratio of the inertial to viscous forces. At low Reynolds number the viscous effects become more prominent and there are many ways to model this phenomenon. Bayt and others had written computational fluid dynamics codes (CFD) in an attempt to create two and three dimensional numerical solutions to the Navier-Stokes equations. Another approach is the DSMC approach which goes behind the continuum assumption and seeks to model the gas on a molecular level. These methods are complicated and often unreliable and one of the goals of this research is to see if a simple quasi one dimensional (1D) approach can provide meaningful insights into the flow behavior. The approach taken is to use the influence coefficients for quasi 1D flow as outlined by Shapiro [39]. In quasi 1D flow the changes in only one coordinate are considered to be significant and the flow is assumed uniform in the other two. For a nozzle it is assumed that the change in cross sectional area is

slow enough such that the flow is uniform in the plane perpendicular to the axial direction. The influence coefficients relate how properties of the flow change with respect to independent variables. They are a set of differential equations that are added together to quantify how a dependent variable changes with a collection of independent properties. For example, the influence of area change on the Mach number squared is;

$$\frac{dM^2}{M^2} = -\frac{2(1+\frac{\gamma-1}{2}M^2)}{1-M^2}\frac{dA}{A}. \tag{2.4}$$

For the case of the micronozzle, the relevant independent variables are Mach number (M), flow velocity (u), temperature (T), total temperature (T_t), pressure (P), and total pressure (P_t). The independent parameters are area change (dA), heat addition (dq) and friction (f). The following equations are generated from the influence coefficients tabulated by Greitzer et al. [14], reproduced from Fitzgerald, [11];

$$\frac{dM^2}{M^2} = -\frac{2(1+\frac{\gamma-1}{2}M^2)}{1-M^2}\frac{dA}{A}+\frac{(1+\frac{\gamma-1}{2}M^2)(\gamma M^2+1)}{1-M^2}\frac{dq}{c_pT_t}+\frac{(1+\frac{\gamma-1}{2}M^2)(\gamma M^2)}{1-M^2}4f\frac{dx}{D}, \tag{2.5}$$

$$\frac{du}{u} = -\frac{1}{1-M^2}\frac{dA}{A} + \frac{(1+\frac{\gamma-1}{2}M^2)}{1-M^2}\frac{dq}{c_pT_t} + \frac{(\gamma M^2)}{2(1-M^2)}4f\frac{dx}{D}, \tag{2.6}$$

$$\frac{dT}{T} = \frac{(\gamma-1)M^2}{1-M^2}\frac{dA}{A} - \frac{(1+\frac{\gamma-1}{2}M^2)(\gamma M^2-1)}{1-M^2}\frac{dq}{c_pT_t} - \frac{\gamma M^4(\gamma-1)}{2(1-M^2)}4f\frac{dx}{D}, \tag{2.7}$$

$$\frac{dTt}{Tt} = \frac{dq}{c_pT_t}, \tag{2.8}$$

$$\frac{dP}{P} = \frac{\gamma M^2}{1-M^2}\frac{dA}{A} - \frac{(1+\frac{\gamma-1}{2}M^2)(\gamma M^2)}{1-M^2}\frac{dq}{c_pT_t} - \frac{\gamma M^2[1+(\gamma-1)M^2]}{2(1-M^2)}4f\frac{dx}{D}, \tag{2.9}$$

$$\frac{dPt}{Pt} = -\frac{\gamma M^2}{2}\frac{dq}{c_pT_t} - \frac{\gamma M^2}{2}4f\frac{dx}{D}, \tag{2.10}$$

where c_p is the specific heat at constant pressure, dx is the change in the x direction and D is the hydraulic diameter. The hydraulic diameter is defined as [45];

$$D = \frac{4A}{P}, \tag{2.11}$$

where A is the area and P is the wetted perimeter. The friction factor is estimated with two different models for flow. For laminar flow in a smoother circular pipe the friction factor is estimated to be inversely proportional to the Reynolds number;

$$f = 64/Re. \tag{2.12}$$

The modified Blasius equation for turbulent flow through smooth rectangular channels is used as the other model [43][21];

$$f = 0.085Re^{-.25}. \tag{2.13}$$

The propellant is assumed to be Hydrazine at 12 atm, 879 degrees K, γ is 1.37, viscosity is 3.38×10^5 kg/m/s, and the mean molecular weight is 10.74 g/mole. This is calculated with the thermodynamic chemical equilibrium calculator Gaseq [34].

The influence coefficients are integrated with Matlab starting from the throat region of a 15 degree cone expansion nozzle. (See Appendix B for code.) The initial Mach number, total Pressure and Temperature are defined and the back pressure is assumed zero to avoid any issues with shocks in the fluid. Furthermore the Reynolds number and Knudsen number (Kn) are calculated from the pressure, temperature, velocity, viscosity and Mach number. The Knudsen number is the ratio of the mean free path of the fluid (λ) to the characteristic length scale of interests (L). The mean free path is the average distance between collisions in the fluid and the characteristic length is any dimension of interest. In the case of a nozzle the throat or nozzle width is used. A small Kn means that many collisions will occur across the throat and the fluid will behave as a continuum, as opposed to a large Kn, where it behaves as a kinetic gas where the trajectories of individual particles must be known to characterize the flow. This can be written as [44];

$$Kn = \frac{\lambda}{L} = \sqrt{\frac{\gamma\pi}{2}}\frac{M}{R_e}. \tag{2.14}$$

As a result it is straight forward to find and plot the Kn with the Mach and Reynolds number solved.

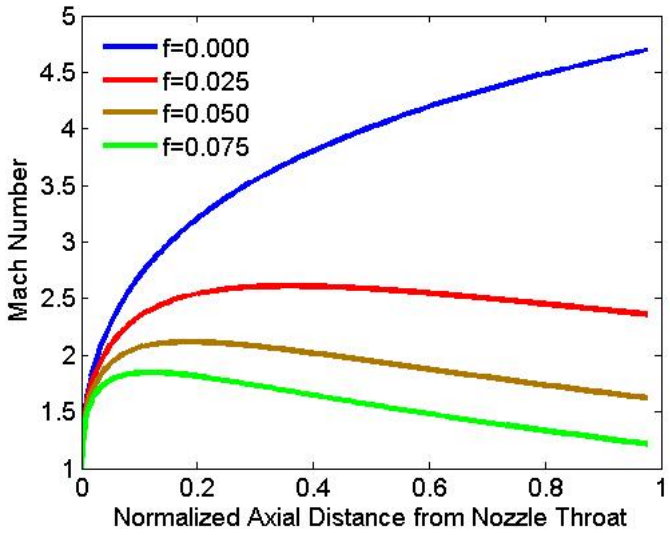

Figure 2-1: Mach Number versus Normalized Axial Distance from the Nozzle Throat

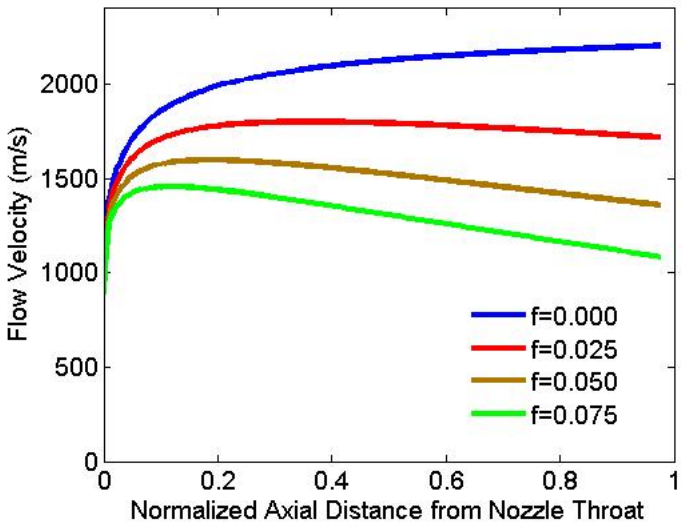

Figure 2-2: Flow Velocity versus Normalized Axial Distance from the Nozzle Throat

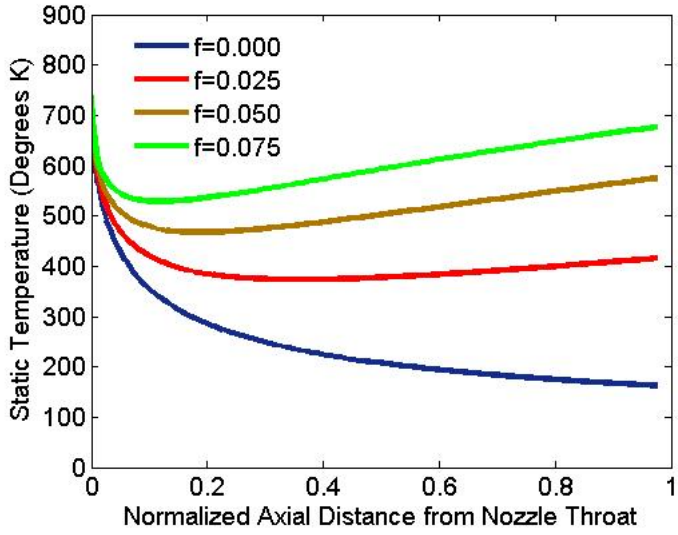

Figure 2-3: Static Temperature versus Normalized Axial Distance from the Nozzle Throat

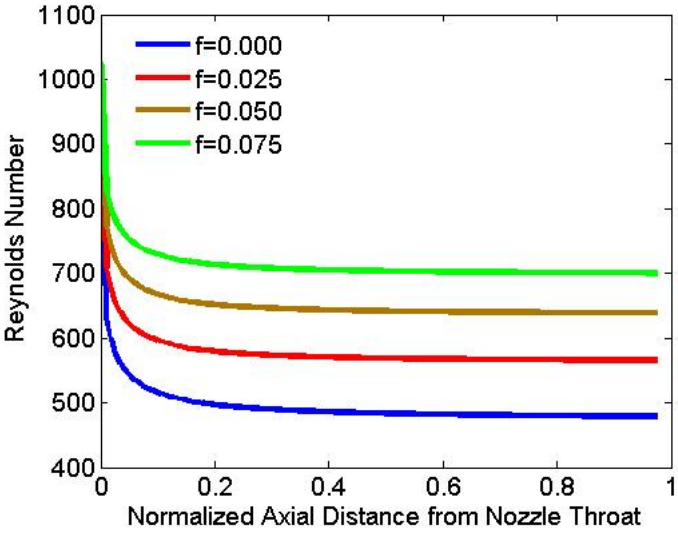

Figure 2-4: Reynolds Number versus Normalized Axial Distance from the Nozzle Throat

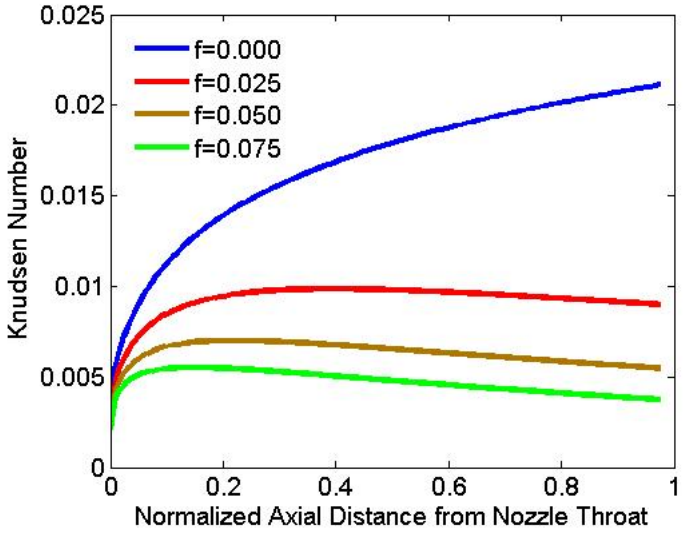

Figure 2-5: Knudsen Number versus Normalized Axial Distance from the Nozzle Throat

The most important observation from the solutions is that the optimal value for Mach number and flow velocity is not at the end of the nozzle when friction is accounted for. Conceptually the "drag" caused by friction overwhelms the expansion process and reduces the Mach number and flow velocity. The graph of Mach number shows a drastic (factor of 3) reduction in Mach number for medium and high values of friction. This is deceptive as the friction increases the temperature in addition to slowing the flow down. Mach number is the ratio of the flow velocity to the local speed of sound which equals,

$$M = \frac{V}{\sqrt{\gamma RT}}, \tag{2.15}$$

where R is the gas constant. Essentially the Mach number is proportional to the Velocity and inversely proportional to the square root of the temperature. The flow velocity only is reduced by at most a factor of two due to friction. The implication of these graphical solutions, is that the nozzle can be optimized by cutting it off roughly 25% downstream of the throat since that part of the expansion is a loss. As a result of this hypothesis, it is decided that any nozzle that is tested is built in three different lengths, a complete expansion, and two nozzles cut short (25 and 50 %). This tests whether a basic influence coefficient analysis is sufficient in predicting

nozzle efficiency. A similar influence coefficients analysis was completed by Dr. Jerry Guenette during the initial phase of the project and similar recommendations were made [16]. Dr. Guenette's work inspired this analysis and the calculations in this thesis go beyond friction and allow for heat addition which is used later.

It is also interesting to observe the Reynolds and Knudsen number behavior along the nozzle. The Reynolds goes down and levels off around 500 without friction when starting at 1,000. It is interesting that it goes down along the nozzle since the flow accelerates and the width increases. However, the density decreases faster than the velocity which drives the Reynolds number down. The Knudsen number steadily rises without friction from less than .005 to .02 along the nozzle. With friction it levels off at around .01.

2.3 Reynolds Number Scaling

The micronozzle is estimated to have a throat width on the order of 35 microns which requires MEMS fabrication. Access to a MEMS fabrication process is outside the budget of this endeavor; however, building upscale nozzles and operating them at sub atmospheric pressures is within the capabilities of the Space Propulsion Lab. The Reynolds number is to be held the same and recalling the definition and applying the ideal gas law and the throat velocity;

$$Re = \frac{\rho U D}{\mu} = \frac{\frac{P_*}{RT_*}\sqrt{\gamma R T_*} D}{\mu} \propto \frac{1}{\sqrt{R}} \propto \sqrt{\bar{M}}, \tag{2.16}$$

where ρ_* and T_* are the conditions at the throat and $\bar{M}$ is the molecular mass. This means that gases with low molecular weight will have lower Reynolds numbers and furthermore its directly proportional to the chamber Pressure. For an upscale nozzle, the chamber temperature is room temperature (300 K) and Helium is used as the working fluid due to its low molecular weight. Helium has a molecular weight of 4 $\frac{g}{mole}$ which is nearly a factor of 5 lower than Nitrogen, the next readily available fluid. The smallest possible throat that can be manufactured is approximately 500

microns and the target chamber pressure for the micronozzle is 10 atm. The quasi 1D isentropic relations for density and temperature are used to find the pressure required for the experiment,

$$\frac{\rho_*}{\rho_0} = \left(\frac{2}{1+\gamma}\right)^{\frac{1}{(\gamma-1)}}, \tag{2.17}$$

$$\frac{T_*}{T_0} = \frac{2}{1+\gamma}. \tag{2.18}$$

Chamber pressures ranging from .05-.75 atm are appropriate for the range of Reynolds numbers to be studied (100-1,400).

2.4 Nozzle Geometries

There are a variety of nozzle geometries that are used throughout the space propulsion community for macroscopic nozzles. The simplest is a 15 degree cone from the center line for a total angle of 30 degrees. This assumes the flow is quasi 1D and is often used when advanced contours are not feasible. A more sophisticated design is a contour that assumes 2D flow. For a cylindrical nozzle, if the radius of curvature is small compared to the contour, then this is a good approximation. For a 2D nozzle cut into a solid surface, if the aspect ratio (nozzle height divided by width) is large then this assumption is also valid. The continuity and momentum equations can be solved numerically in curvilinear coordinates to create a contour for isentropic 2D expansion, and this is used to design another type of nozzle to be tested. The third contour design takes a first order approximation of the frictional effects. The flow in between the boundary layers is assumed to be isentropic. The nozzle contour is then widened such that the edge of the boundary layer is the contour for the ideal 2D flow case. (This idea was inspired during personal communication with Professor Martinez-Sanchez [31].) The displacement thickness represents how an external streamline in a fluid flow is displaced due to a boundary layer. It is defined to be for a compressible fluid;

$$\delta* = \int_0^\infty \left(1 - \frac{\rho(y)u(y)}{\rho_e u_e}\right) dy \tag{2.19}$$

where $\rho(y)$ and $u(y)$ are the density and velocity parallel to the surface (x direction), and ρ_e and u_e the values just outside the boundary layer in the inviscid region. The calculation for the 2D flow is done with the Method of Characteristic as outlined by Martinez-Sanchez [29] and Thompson [42]. The method starts with an inlet supersonic flow near Mach one that expands isentropically through a sharp corner. This occurs through a theoretically infinite number of expansion waves known as Prandtl-Meyer expansion waves [1]. This numerical method breaks that process into a finite number of waves. The Prandtl-Meyer function is solved for the exit and inlet Mach numbers and then divided into invariant Mach waves.

$$\nu(M) = \sqrt{\frac{\gamma+1}{\gamma-1}}\tan^{-1}\left(\sqrt{\frac{\gamma-1}{\gamma+1}(M^2-1)}\right) - \tan^{-1}(\sqrt{M^2-1}) \tag{2.20}$$

Along each invariant the flow properties are assumed constant. The Prandtl-Meyer function and the flow angle (θ) can then found from the invariants;

$$\nu(M) = \frac{I_2^+ - I_2^-}{2}, \tag{2.21}$$

$$\theta = \frac{I_2^+ + I_2^-}{2}. \tag{2.22}$$

The Mach number for each Mach wave intersection can then be found from solving the Prandtl-Meyer function. The Mach angle is then calculated from the Mach number;

$$\mu = sin^{-1}\frac{1}{M}. \tag{2.23}$$

The flow angle and the Mach angle can then be used to find the intersection of the Mach waves depicted in the following figure.

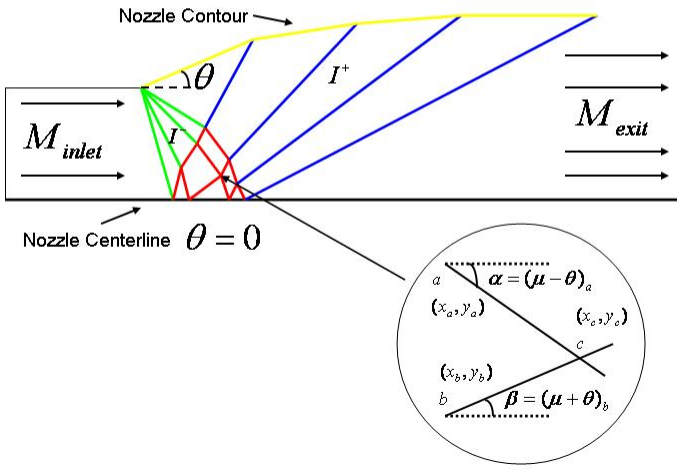

Figure 2-6: Diagram of 2D Prandtl-Meyer Expansion Process

The green and blue regions represent simple regions with negative and positive Invariants respectively. The red region represents the nonsimple region where the mach waves intersect. This is where some cumbersome trigonometry is used to find the location of all the intersections. The intersection of the positive invariants with the flow angle allowed the contour to be calculated. Furthermore the throat is assumed to be unity or a normalized value since that is arbitrary. One of the contributions of this thesis is a free code that allows one to calculate the nozzle contour with a user defined number of expansion waves. It is reasonable to obtain rough estimates using 4 waves and calculating the points by hand; however, that becomes impractical for more waves. The code written does some averaging of the flow angles to improve the numerical accuracy as well. See appendix A for the code.

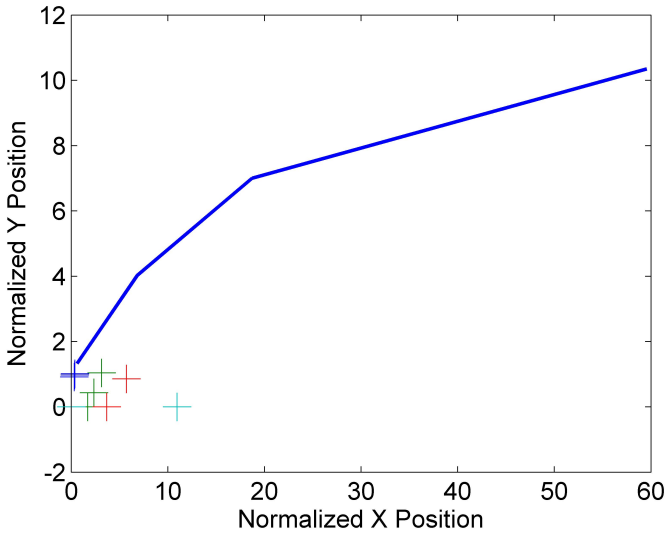

Figure 2-7: Nozzle Contour from Mach 1 to 4.8 via Method of Characteristics with 4 Expansion Waves

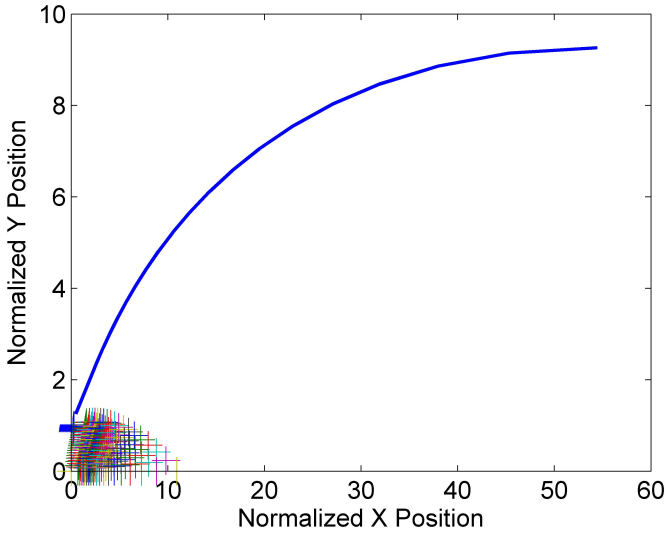

Figure 2-8: Nozzle Contour from Mach 1 to 4.8 via Method of Characteristics with 20 Expansion Waves

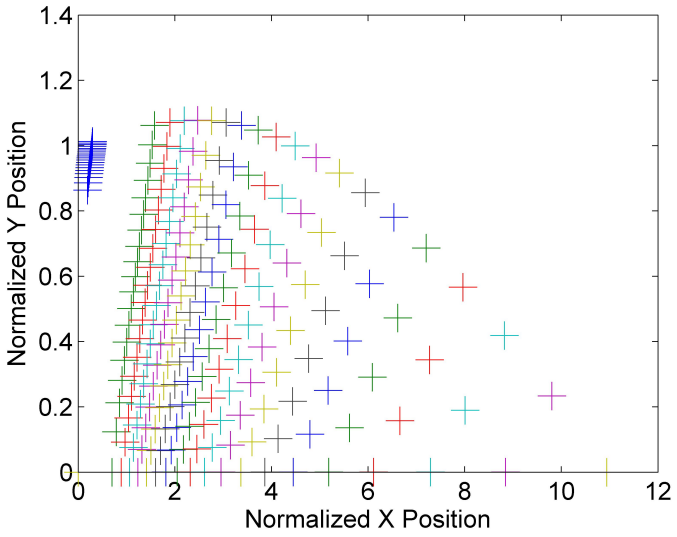

Figure 2-9: Zoomed in View of the 20 Expansion Wave Intersections

The nozzle contour for an expansion from Mach 1 to 4.8 is shown in figure 2-7 and 2-8. The contour generated with 20 waves is much smoother than with 4 and that contour is assumed to be ideal. The expansion wave intersections are difficult to see on the plot and they represent the red non simple region. A zoomed in view is shown for clarity. The displacement thickness is then calculated and a wider nozzle is calculated. The calculation was done by Professor Mark Drela and the ideal contour is assumed to be a streamline for the inviscid region [9]. The new contour is graphed next to the ideal.

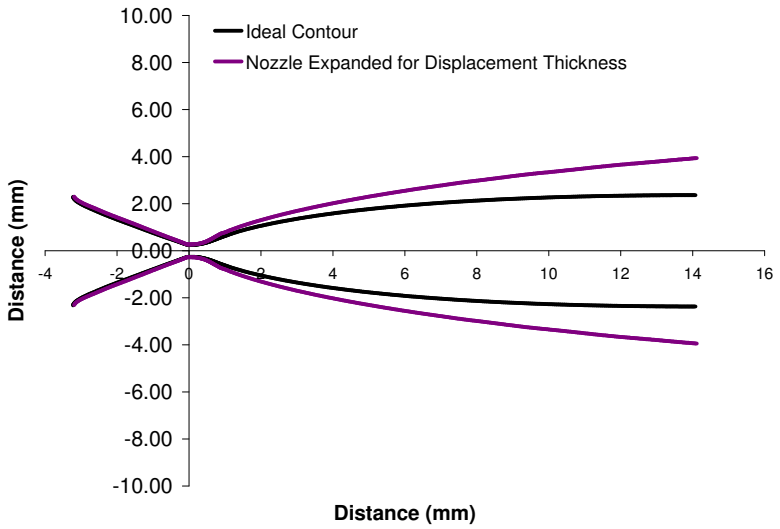

Figure 2-10: Nozzle Contour with Displacement Thickness

This leads to three different classes of nozzles that are built and tested, and each nozzle is cut at three different axial lengths, 25, 50 and 100 %. One of the primary experimental goals is to see if cutting the nozzle shorter can improve the thrust efficiency. Furthermore determining if improvements to a 15 degree expansion provides practical data for propulsion engineers. Specifically if no noticeable improvement is attained with a contour generated with 2D numerical simulation or a widened nozzle, then simpler geometries can be built. This is particularly relevant for cooling the perimeter of the nozzle where complicated contours provide fabrication challenges.

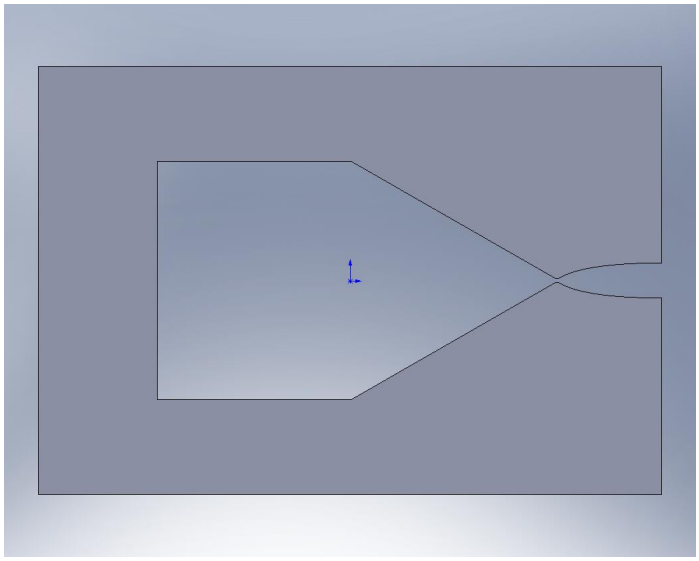

Figure 2-11: Ideal Contour, 100% Axial Length, Entire Nozzle Cross Section

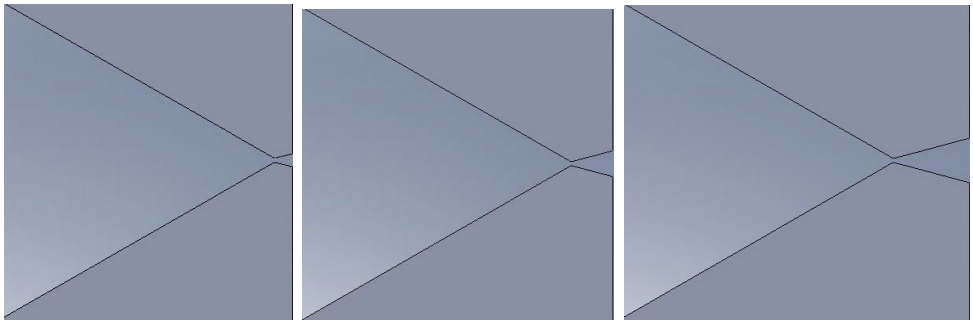

(a) 25% Axial Length (b) 50% Axial Length (c) 100% Axial Length

Figure 2-12: Expanded View, 15 Degree Cone Nozzles

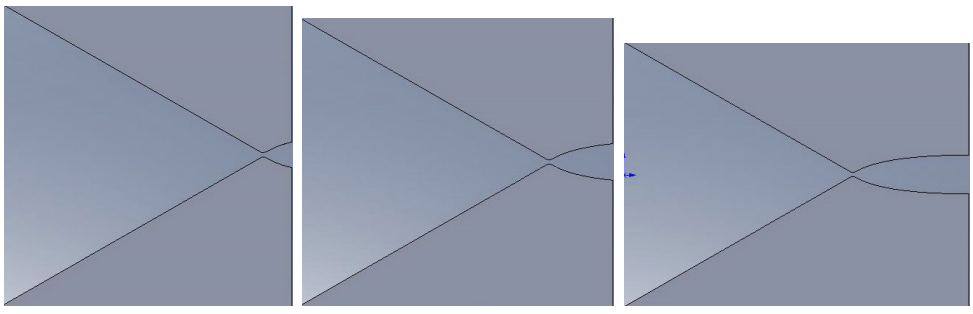

(a) 25% Axial Length (b) 50% Axial Length (c) 100% Axial Length

Figure 2-13: Expanded View, Ideal Contours

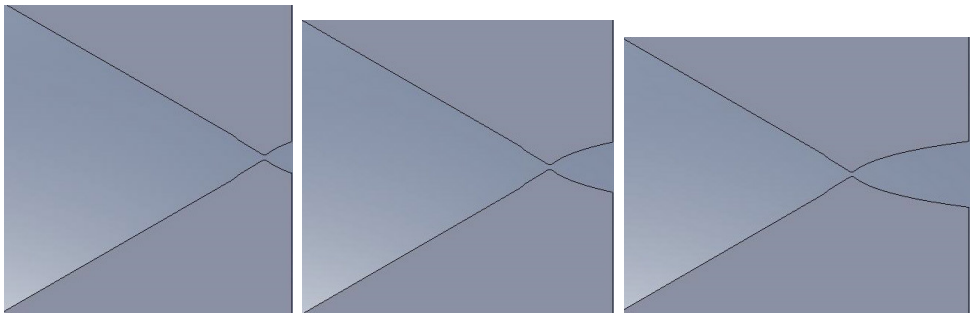

(a) 25% Axial Length (b) 50% Axial Length (c) 100% Axial Length

Figure 2-14: Expanded View, Ideal Contour Widened for Displacement Thickness

Chapter 3

Experimental Work

3.1 Nozzle Fabrication

The nozzles are manufactured with polycarbonate since it is strong, machinable and transparent. The polycarbonate is cut out on the MIT Aerospace's department waterjet, (OMAX 2652 JetMachining Center [7]). The nozzles are made from five layers that are "plexiglass welded" together [6]. The middle layer is 1/8 of an inch or approximately 3 mm thick, and it has the contour of the nozzle cut in it. The nozzles have a "settling" chamber which is a place where the gas can dissipate its momentum after leaving the inlet prior to entering the converging section. Two pieces of 1/8 inch polycarbonate with a rectangular hole cut in them are attached to the center nozzle piece. 1/8 inch is chosen to provide ample room for the pipe fittings to be screwed into the nozzle. The two 1/4 inch flat plates are welded on each end to seal the nozzle.

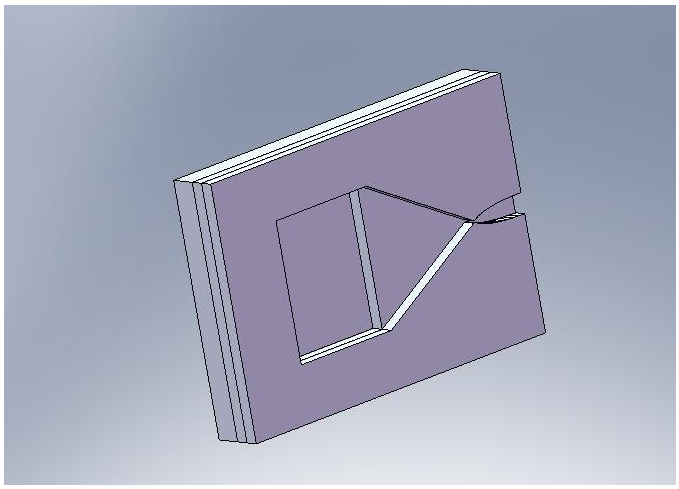

Figure 3-1: View of Nozzle Polycarbonate Layers

The nozzle manufacturing process is as follows:

1. SolidWorks drawings are made and the files are edited for the OMAX software.

2. The Polycarbonate is cutout on the waterjet.

3. The pieces are carefully sanded and measured with a caliper to check precision.

4. Each piece is cleaned with alcohol and they are then welded together.

5. The nozzles are compressed in a vice to dry properly for 24 hours.

6. The edges are carefully milled to make the nozzles square.

7. 1/4 and 1/8 inch pipe threads are tapped into the nozzle.

8. The nozzles are cleaned multiple times with isopropyl and ethanol alcohol to prevent out-gassing in vacuum.

9. 1/4 and 1/8 inch Swagelok fittings are screwed into the nozzle for the Helium inlet and Pressure Transducer.

Figure 3-2: Example of Fabricated Nozzle

Each nozzle throat is measured by carefully placing the rear end of drill bits into the throat. The drill bits are measured with a precision micrometer and this technique allows for measurements to half a thousandth of an inch. (In excess of 30 nozzles were built over several months since it took a few trials to get everything to work.) It is a tedious process and requires care when sanding, welding and milling. In total, ten nozzles are built for testing. In addition to the nine nozzles discussed previously, an extra 2D Ideal 100% axial length nozzle is built from 1/4 inch polycarbonate as opposed to 1/8 inch to see if the effect of the endwall displacement thickness can be reduced.

Throat Width (m)	Nozzle
5.33×10^{-4}	15 Degree Cone 25% Axial Length
5.08×10^{-4}	2D Ideal 25% Axial Length
5.33×10^{-4}	2D Ideal with $\delta * 25\%$ Axial Length
5.33×10^{-4}	15 Degree Cone 50% Axial Length
5.33×10^{-4}	2D Ideal 50% Axial Length
5.33×10^{-4}	2D Ideal with $\delta * 50\%$ Axial Length
4.57×10^{-4}	15 Degree Cone 100% Axial Length
5.08×10^{-4}	2D Ideal 100% Axial Length
5.08×10^{-4}	2D Ideal with $\delta * 100\%$ Axial Length
5.33×10^{-4}	2D Ideal 100% Axial Length (1/4" Thick)

Table 3.1: Nozzle Throat Dimensions

3.2 Experimental Apparatus

The experiments are carried out in the MIT Space Propulsion Lab in the AstroVac vacuum chamber. The basic process of the experiment is to flow room temperature gas through a low pressure, up scale nozzle in a large vacuum chamber and measure the chamber pressure and thrust. In order for this to be a valid experiment, the tank must be large with respect to how much gas is released into the tank to maintain near vacuum conditions. AstroVac is approximately 2 m^3 and the maximum mass flow is on the order of 10^{-4} kg/s which leads to an ambient pressure of approximately .01 atm using Helium for approximately 30 seconds. This is not ideal, but tolerable since the ambient pressure (P_a) is the same order of magnitude as the exit pressure of the nozzle and needs to be accounted for in the thrust calculations. The Vacuum chamber is equipped with multiple ports; however, two are available for this gas flow. One port is an inlet for Helium into the nozzle and the other port is a static line for the pressure transducer. This line measured the nozzle "settling" chamber pressure. The Vacuum chamber does have a pressure measurement system for the ambient

pressure; however, it only works with air since it uses the resistivity of the gas to calculate pressure. Helium is not compatible with the gauge and this presents a small difficulty to be described later in determining the ambient pressure. A high precision test stand was built for the lab and is used to measure the thrust of the nozzle. The stand was originally built by Jareb Mirczak in 2003 [33] and then made operational by Randy Leiter in 2009 [24]. It has a range of approximately 100 mN with less than 1 % error [24]. The stand is a torsional balance thrust measurement system with a central pivot arm that balances the thrust force with an applied force.

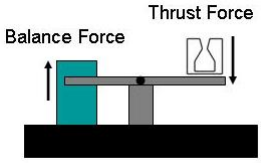

Figure 3-3: Torsional Balance Arrangement for Test Stand

The nozzle sits at one end and expels gas upward providing a down force. The stand then is balanced by a BEI LA10-08-000A voice coil to provide a counter force and its position is measured with a linear variable differential transducer (LVDT) [33]. A PID control system is interfaced with LabView software to create a user friendly interface [24].

Item	Specification
Pressure Transducer	Omega PX209, 0-30 Bar pressure, 0-5 Vdc output
Volt Meter	find item
Power Supply	find item
Vacuum Chamber	MIT SPL AstroVac, (10^{-3} - 760) Torre, $\approx 2m^3$
Thrust Stand	MIT SPL Custom built stand, (0-100) mN

Table 3.2: Summary of essential equipment

Below are photos and a diagram of the experimental setup.

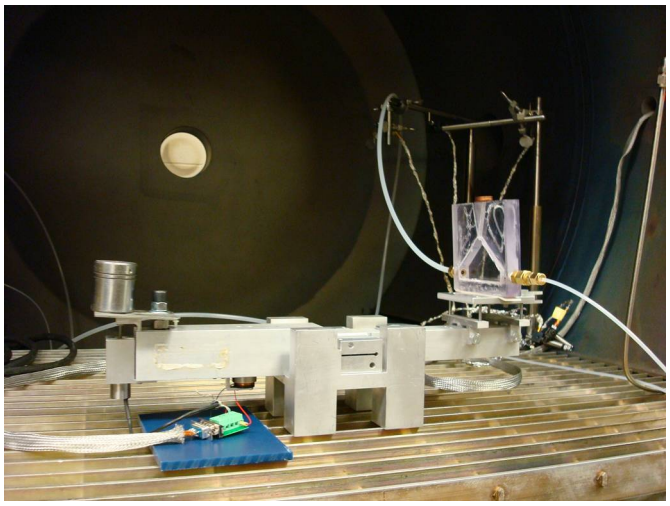

Figure 3-4: Experimental Setup, Inside Vacuum Chamber, Test Stand with Nozzle Attached

Figure 3-5: Experimental Setup, Outside Vacuum Chamber, Ports for Helium and Pressure Line, and Pressure Transducer with Volt Meter

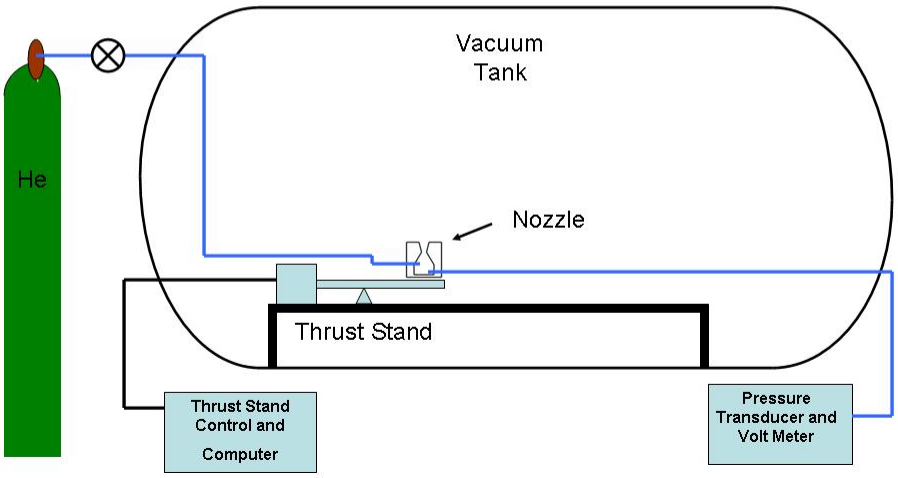

Figure 3-6: Experimental Setup Overview

3.3 Experimental Procedure

The experiments are done in continuous runs for each nozzle. The lab is shared among many experiments and as a result this experiment needs to be reset up for each experiment. The following is the experimental procedure:

1. The nozzles and feedlines are thoroughly cleaned with alcohol to prevent outgassing in the vacuum system.

2. The feedlines are Swagelok attached to the nozzle carefully without kinking the lines or applying strong torques.

3. The nozzle is taped to the stand with double sided tape and the gas lines are placed in a relaxed position.

4. The test stand computer is turned on but not actively controlled so the stand can freely move.

5. The stand is then carefully balanced with counter weights.

6. The control system is then activated and the stand is then being actively held level.

7. The stand is calibrated by placing five USA pennies one at a time on the nozzle exit. US pennies weigh precisely 2.5 grams [41] and this calibration has to happen with every new nozzle.

8. The pennies are removed and the stand position should return to zero and no force should be applied in steady state. If this is not true the initial balance with no active control needs to be repeated and then a redo of the calibration.

9. The barometric pressure is recorded and the pressure transducer is also recorded to provide a data point for it's calibration.

10. The vacuum chamber is closed and pumped down. Inevitably the lines shift their position some due to evacuation of their internal gas from ambient conditions.

11. Once in vacuum (mili-tor range) the voice coil's force is read to provide a baseline for the thrust readings to account for any forces the shift in the feedlines causes.

12. The pressure gage on the tank is recorded since it is assumed accurate since the ambient gas is air not Helium.

13. The pressure transducer is recorded to provide a calibration point at vacuum conditions.

14. Data is taken, see below.

15. The voice coil force is recorded to check for drift.

16. The stand is turned off and the tank is opened.

The procedure for each tests is as follows:

1. The Helium line is cracked open and the pressure in the nozzle is monitored. The pressure is increased until it reaches the target pressure which ranges from approximately 70 kpa to 5 kpa depending on the test.

2. The chamber pressure is recorded and once the stand is level the thrust is recorded.

3. The Helium line is then shut as quickly as possible.

4. As the Helium in the line runs into the nozzle, the pressure will still show a substantial reading. It takes approximately 5 minutes for the pressure to reach steady state and at this time the pressure inside the nozzle is the same as the ambient pressure. This pressure is recorded and is considered the ambient pressure in the tank. The volume of Helium in the line is small compared to the tank volume so the extra Helium added to the tank between thrust reading and ambient pressure reading is negligible.

5. The tank is pumped down for the next run.

The entire cycle takes between 20 and 30 minutes primarily due to the pump down times. This means at most 15 data points can be recorded in an evening. Two or three data points are taken near throat Reynolds numbers of a 1,000 to provide additional data.

Chapter 4

Experimental Results and Error Analysis

4.1 Thrust Data

The most direct results are the thrust data. The thrust is taken directly from the stand after fitting the raw data to a calibration curve. The stand has an error of approximately 1 % or 0.0014 N [24]. The Reynolds number is calculated from the chamber pressure via equation 2.16.

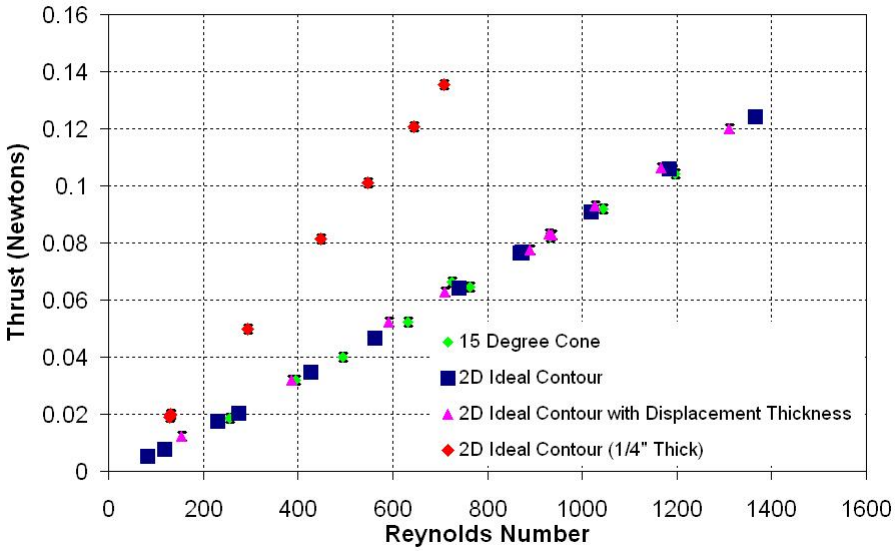

Figure 4-1: Thrust versus Reynolds Number for Nozzles with 100% Axial Lengths, with Error Bars for Thrust

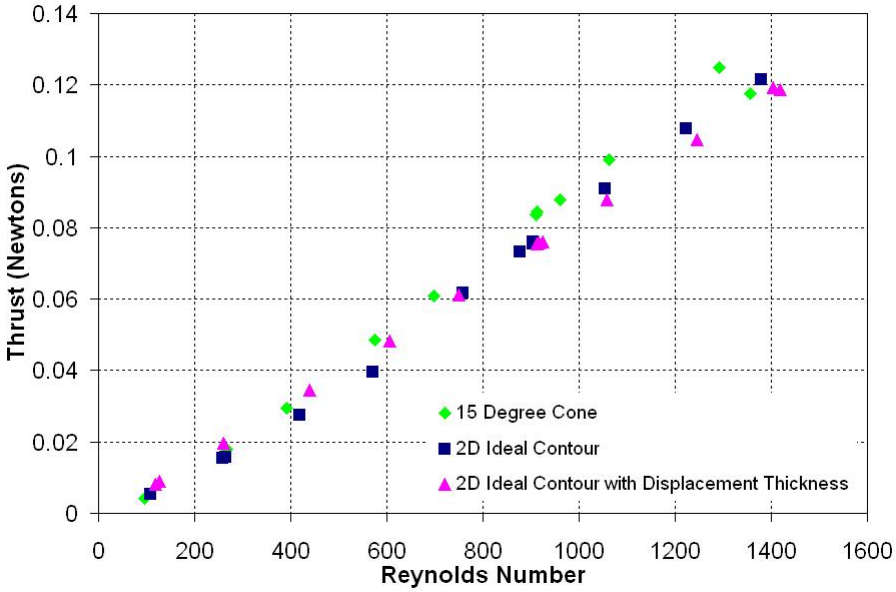

Figure 4-2: Thrust versus Reynolds Number for Nozzles with 50% Axial Lengths

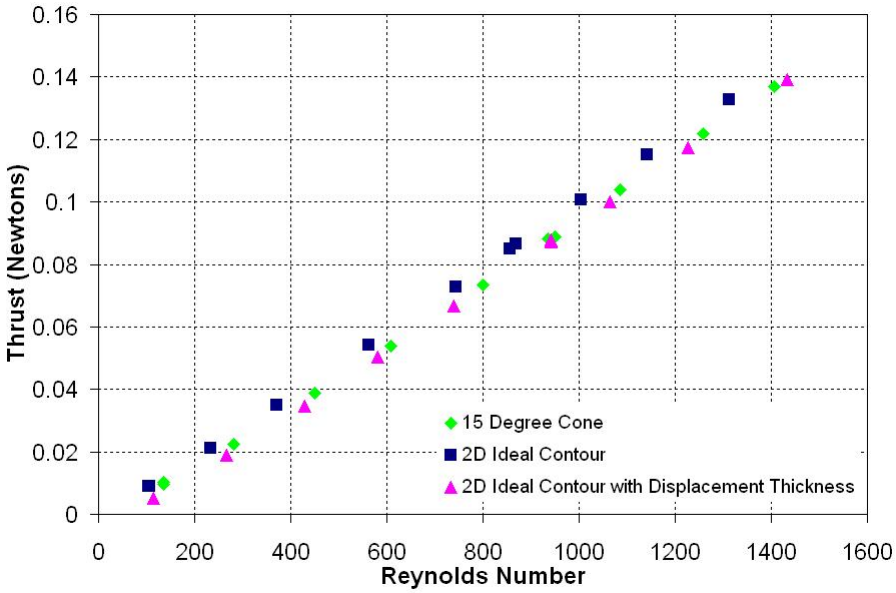

Figure 4-3: Thrust versus Reynolds Number for Nozzles with 25% Axial Lengths

The thrust error is small and is shown only on the first graph. The data is peculiar in that there is no significant difference between the 15 degree cone, 2D ideal contour and the 2d ideal contour with a displacement thickness. The red line in the first graph is the 1/4" thick nozzle which has twice the mass flow rate so it should have twice the thrust, which is does. Furthermore there is little noticeable difference between the three classes of nozzles for 100-25% expansion. There is an approximate increase of 20 mN for the 25% at Reynolds numbers of 1,400. This is small and the data is examined for thrust efficiency to observe any improvements between the cases.

4.2 Thrust Efficiency Results

The thrust efficiency is calculated by dividing equation 2.2 by 2.3. The pressure ratio is calculated assuming isentropic flow. That is an assumption in the equations which is clearly questionable; however, it is a theoretical maximum. Furthermore a detailed error analysis is done to analyze this data. The most significant contribution to error is the measurement of ambient pressure at low pressures. The pressure transducer is at best accurate to ±500 Pascals [10] which limits the quality of the results severely

at Reynolds numbers below 500. The error bars are substantial and included in all the plots.

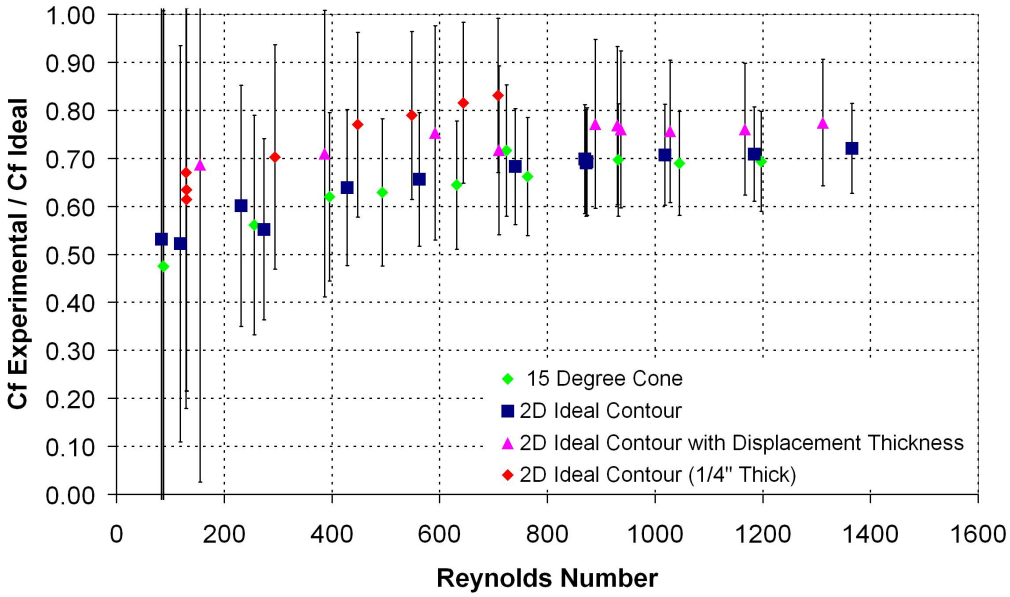

Figure 4-4: Thrust Efficiency versus Reynolds Number for Nozzles with 100% Axial Lengths. Error Bars are included.

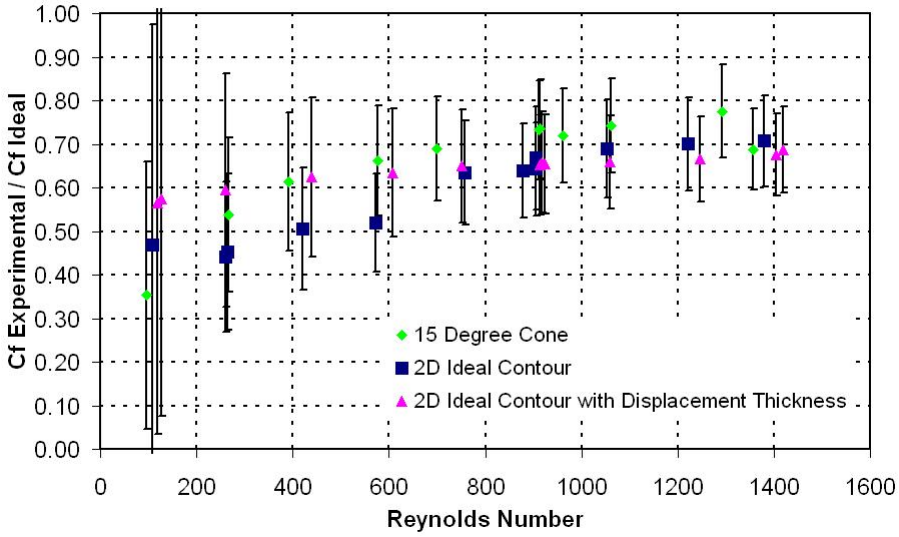

Figure 4-5: Thrust Efficiency versus Reynolds Number for Nozzles with 50% Axial Lengths. Error Bars are included.

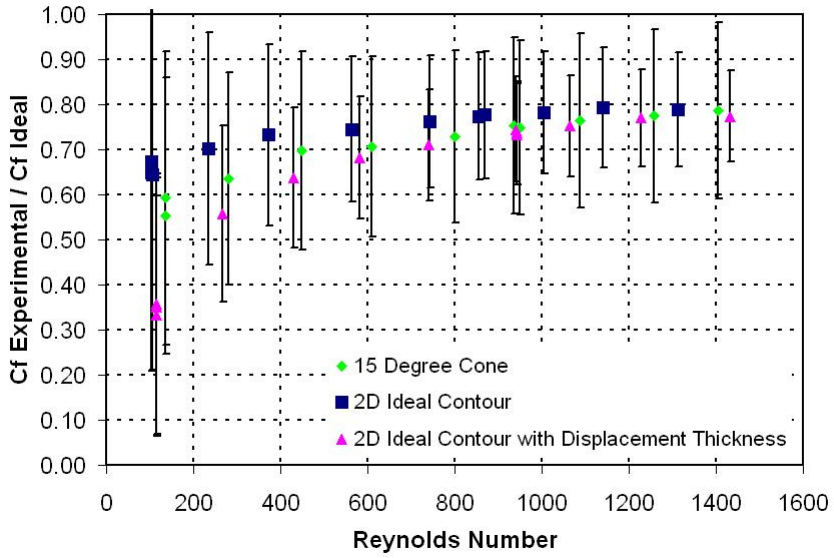

Figure 4-6: Thrust Efficiency versus Reynolds Number for Nozzles with 25% Axial Lengths. Error Bars are included.

The thrust efficiency is more complicated and changes significantly for different Reynolds numbers. As per the thrust plots there is no significant difference in effi-

ciency between the 15 degree cone, 2D ideal contour and the 2D ideal contour with a displacement thickness. The only nozzle to show a noticeable improvement is the 1/4" thick 2D ideal contour. This suggest viscous effects with the end walls is significant with the other nozzles. The other nozzles all show a similar curve with efficiency around 75% for Reynolds numbers above 1,000 and a smooth drop to approximately 50% for Reynolds numbers below 200. There is a slight improvement of about 5% for the shortest nozzles (25% axial length). No improvement is observed for the 50% axial length nozzles. This is very interesting since the displacement thickness starts to account for a large portion of the nozzle approximately 50% axially down the throat in figure 2-10. At (25%) it is negligible and this makes physical sense since the boundary layer grows with the square root of the ratio of viscous to convection diffusion. That can be seen from the diffusion equation;

$$\frac{\partial \chi}{\partial t} = D\nabla^2\chi, \tag{4.1}$$

where D is the diffusion coefficient and χ is any quantity of interests. This equation scales as,

$$\frac{1}{t} \propto \frac{D}{x^2}, \tag{4.2}$$

or

$$x \propto \sqrt{Dt}. \tag{4.3}$$

This means as a general approximation where D is the viscous diffusion coefficient, the boundary layer thickness will grow as;

$$\delta \propto \sqrt{\frac{\mu}{\rho}t}, \tag{4.4}$$

or non dimensionally,

$$\frac{\delta}{x} \propto \sqrt{\frac{\mu}{\rho u x}}, \tag{4.5}$$

where δ is the boundary layer displacement thickness, x is the length scale, μ is the viscosity, ρ is the density and u is the velocity. The meaning that is extracted from

these scaling laws is that for highly accelerating flows the boundary layer growth is small, and for high viscosity or low acceleration the boundary layer is large [31].
In the beginning of the expansion process, the area change is relatively high so convection will dominate and thin the boundary layer. In the later parts of the expansion, the velocity gradient is lower and the viscous effects will become more apparent. It is peculiar that there is no noticeable change in efficiency between the different lengthened nozzles. One hypothesis is the endwall boundary layers, but those also will be similar to the boundary layers along the contours. Another possibility is viscous losses upstream of the throat. This also seems unlikely by the same analysis since the sub sonic region is heavily convective.

Another possible effect is flow separation. If the ambient pressure is too high relative to the exit pressure of the nozzle, the viscosity of the fluid will be insufficient to keep the fluid attached to the nozzle wall and the flow will detach from the nozzle. This happens approximately when the exit pressure is less than 40% the ambient pressure [28]. This detachment will match the exit pressure with the ambient pressure, which effectively reduces the expansion ratio of the nozzle. In the experiments the exit pressure (calculated assuming isentropic flow) is sometimes less than 40% the ambient pressure. As a result, thrust efficiency calculations are redone assuming the flow separates. The ambient pressure is assumed to be the exit pressure and the exit Mach number and area can then calculated. Essentially the calculation leaves everything the same for exit pressures above 40% ambient pressure and for values below, it creates a new thrust coefficient via equation 2.3 with the increased exit pressure.

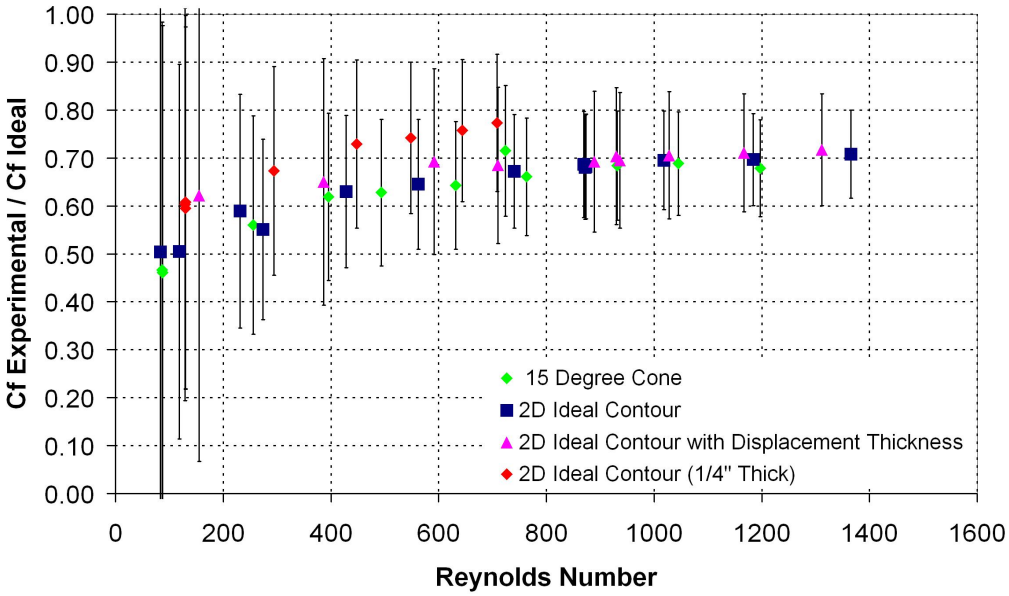

Figure 4-7: Thrust Efficiency Accounting for Flow Separation versus Reynolds Number for Nozzles with 100% Axial Lengths. Error Bars are included.

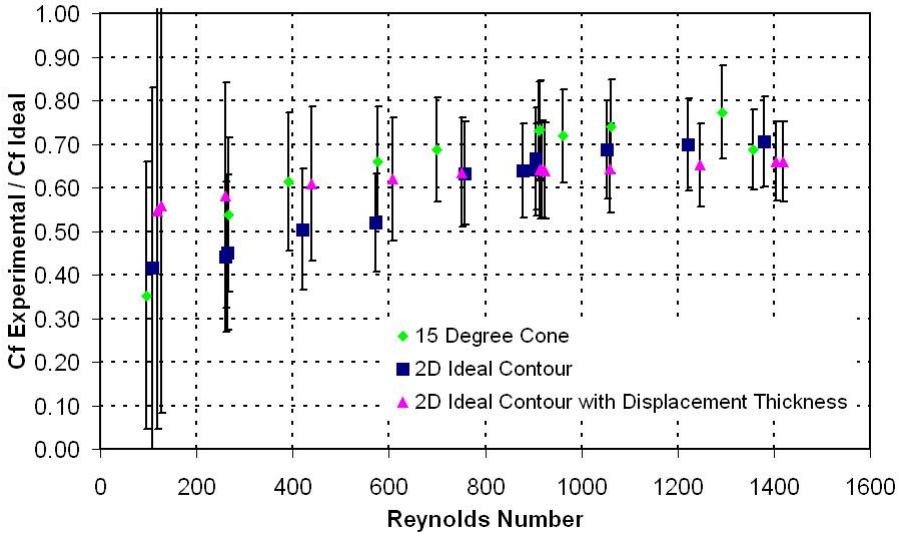

Figure 4-8: Thrust Efficiency Accounting for Flow Separation versus Reynolds Number for Nozzles with 50% Axial Lengths. Error Bars are included.

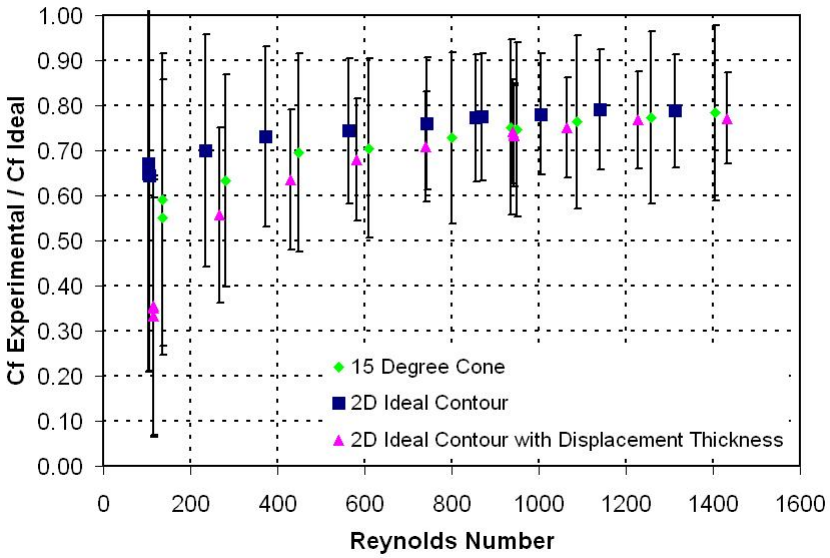

Figure 4-9: Thrust Efficiency Accounting for Flow Separation versus Reynolds Number for Nozzles with 25% Axial Lengths. Error Bars are included.

The efficiency gets worse for the nozzles with a full 100% expansion; however, it improves or stays the same with the shorter nozzles. This is consistent with equation 2.3 since the $(P_e - P_a)A_e$ term is negative and accounting for separation eliminates it, and increases the ideal thrust coefficient. It is unclear whether separation is indeed occurring though since the pressure difference is within a factor of two, of the 40% criteria and the actual exit pressure is likely higher due to viscous effects. Furthermore the effects of separation are small assuming they are true and doesn't explain the efficiency results.

Another possibility is the exit flow angle of the nozzles. All of the nozzles except the 2D ideal contour with and without the displacement thickness, have an exit angle of the flow that is not parallel the axis of the nozzle. This means some of the momentum of the flow is directed perpendicular to the nozzle and is not providing propulsive force. This is a tiny effect though and the largest angle is for the 25% 2D

ideal contour with the displacement thickness, at 20 degrees. The ideal thrust is [17];

$$T = \dot{m}u_e \frac{1 + cos(\alpha)}{2} + (P_e - P_a)A_e, \tag{4.6}$$

where α is the exit angle of the flow. This only reduces the effectiveness of the momentum term by 3% which is negligible.

Heat transfer is another possible loss for the nozzle. In the experiments, the flow enters the nozzle at roughly room temperature and the nozzle is assumed isothermal. This means heat will flow into the gas since the gas is cooling as it expands. This will slow the gas down according to the influence coefficient for heat addition in supersonic flow 2.6 and reduce the exhaust velocity. Heat transfer in rocket nozzles involves a lot of analysis and a quick orders of magnitude analysis is done to observe any significant effects. Heat transfer between the wall and the gas is proportional to the difference in temperature between the fluid at the wall and the wall temperature;

$$q_w = h(T_{nozzlewall} - T_{fluidwall}), \tag{4.7}$$

where q_w is the heat flux at the wall, h is the heat transfer coefficient, $T_{nozzlewall}$ is the nozzle wall temperature and $T_{fluidwall}$ is the fluid temperature adjacent to the wall. The fluid temperature is approximated with a 90% recovery factor. The fluid is assumed to stick to the wall and if brought to rest purely adiabatically the wall temperature would be the stagnation temperature. There are losses due to friction and the fluid temperature is calculated using the recovery factor [17];

$$T_{fluidwall} = (T_t - T)r + T, \tag{4.8}$$

where T is the static temperature and r is the recovery factor. One of the challenges in heat transfer is finding the coefficient h. For laminar flow over a flat plate, it is approximated as [46];

$$h = \frac{0.365 Re_x^{\frac{1}{2}} Pr^{\frac{1}{3}} k}{x}, \tag{4.9}$$

where Re_x is the Reynolds number where the length scale is x (the distance the flow moves over), Pr is the Prandtl number and k is the thermal conductivity. When applying a Reynolds number of 12,000, the smallest length scale possible of 1 mm, a Prandtl number of 0.680 [19] and a thermal conductivity of 0.152 W/mK [19], the heat transfer coefficient is roughly 5,300 $W/(m^2K)$. This is used in the influence coefficients code and the dimensions of the actual experiment with Helium gas at 300 K are used. No significant ($< 1\%$) change in flow velocity is observed with h on the order of 5,000 $W/(m^2K)$. It took a heat transfer coefficient of 10,000 $W/(m^2K)$ to make a noticeable difference. As a point of reference, macroscale rockets have h values, ($\sim 10^5$ $W/(m^2K)$) [30], which is only an of magnitude above what the influence coefficients predict are necessary to be significant. The flow velocity is plotted with and without heat addition to show its effects.

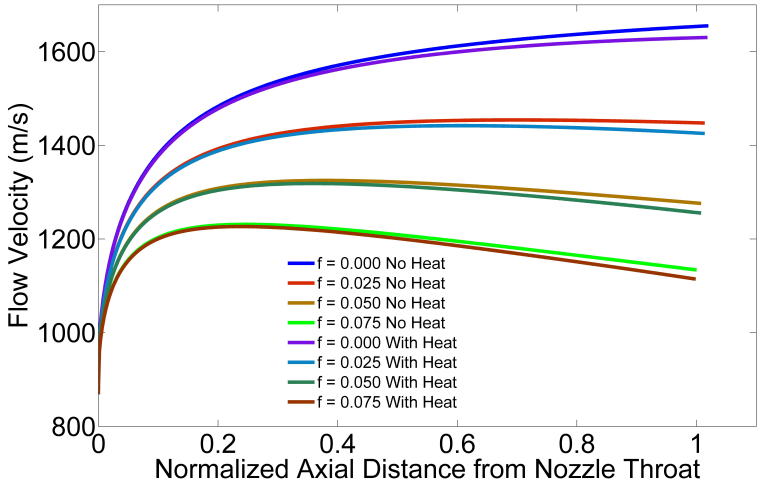

Figure 4-10: Flow Velocity versus Normalized Axial Distance from the Nozzle Throat with Heat Addition and Friction

It is likely heat transfer is not a significant factor in the results since it requires a factor of two increase over the laminar plate model to show a noticeable change. Furthermore the Reynolds number and length scale in the laminar plate calculation were all estimated to maximize h and relaxing those assumptions yields an h of about 1,000 $W/(m^2K)$, which is well below what is predicted to be significant. This analysis is far from rigorous and a more detailed analysis might explain some of the losses

observed in the experiment.

Overall, the data is consistent with the plots of velocity verse axial length 2-2 and Mach number verse axial length 2-1. Specifically if the friction factor is around 0.025, then the velocity does not drop more than 10% along the nozzle. This suggest that viscous losses may not be very important for Reynolds numbers around 1,000. The 80% thrust efficiency requirement is demonstrated at Reynolds numbers above 600 which experimentally verifies that such nozzles can be operated with reasonable efficiency. This is done with the 1/4" thick 2D ideal contour and the other contours are approximately 10% lower at a given Reynolds number. The error bars are approximately 10% at higher Reynolds numbers, and they quickly increase to almost 50% at lower Reynolds numbers. The error is large; however, there is consistency in the results and it is reasonable for engineers to assume greater than 80% efficiency for Reynolds numbers above 1,000. The efficiency takes a consistent fall to below 50% as the Reynolds number is lowered. It is clear viscosity is important in this flow regime and cannot be ignored.

4.3 I_{SP} Efficiency Results

There are two other efficiencies of interest, I_{sp} efficiency and overall performance efficiency. A priori it seems that I_{sp} efficiency should be the same as thrust efficiency since they differ by a constant ($\dot{m}$) when a nozzle is expanded to near vacuum conditions. (Furthermore I_{sp} and exhaust velocity differ by a constant g_0, and exhaust velocity efficiency will be used for convenience.) Since back pressure plays an important role in this experiment, I_{sp} efficiency and thrust efficiency are not equivalent and some analysis is required to observe this. The thrust efficiency is;

$$\eta_{Thrust} = \frac{Thrust_{measured}}{Thrust_{ideal}} = \frac{Thrust_{measured}}{\dot{m}u_{e\,ideal} + (P_e - P_a)A_e}, \tag{4.10}$$

and the exhaust velocity efficiency is;

$$\eta_{u_e} = \frac{u_{e\,measured}}{u_{e\,ideal}}. \tag{4.11}$$

The exhaust velocity is found by subtracting the pressure term from the thrust equation to try to calculate the "actual" velocity of the gas. The exhaust velocity is,

$$u_e = \frac{T_{measured} - (P_e - P_a)A_e}{\dot{m}}. \tag{4.12}$$

The exhaust velocity efficiency then becomes;

$$\eta_{u_e} = \frac{\frac{Thrust_{measured} - (P_e - P_a)A_e}{\dot{m}}}{u_{e\,ideal}}. \tag{4.13}$$

This equation requires knowledge of the exit pressure and mass flow rate. Neither are measured in this experiment and are calculated with isentropic relations. This is a guess as to what the values are and exit pressure is likely higher due to friction and the mass flow rate likely smaller. The overall performance efficiency is calculated by simply dividing the measured thrust by the calculated mass flow rate and comparing that value to the ideal exhaust velocity,

$$u_{e\,performance} = \frac{T_{measured}}{\dot{m}}. \tag{4.14}$$

The performance efficiency then becomes;

$$\eta_{Performance} = \frac{\frac{Thrust_{measured}}{\dot{m}}}{u_{e\,ideal}}, \tag{4.15}$$

which is lower than the thrust efficiency as per equation 4.10 since the pressure term is negative, it lowers the denominator and increases the thrust efficiency. The performance efficiency as per equation 4.15 is known as the effective I_{sp} efficiency. From a purely rocket performance perspective, it is the relevant result since that I_{sp} is what is used in the rocket equation 1.4 to calculate mission $\Delta Velocity$. The efficiency

calculated via equation 4.13 is the corrected I_{sp} or exhaust velocity efficiency. This is the more germane result for these experiments since ambient pressure effects are a performance loss of this particular experiment due to a finite tank volume with limited pumping capacity. In space, ambient pressure effects, won't matter as much in a vacuum expansion process. Since the experiment is unrealistic in this regard, it is best to account for this in the efficiency calculation. To be rigorous the results for both types of efficiency are plotted.

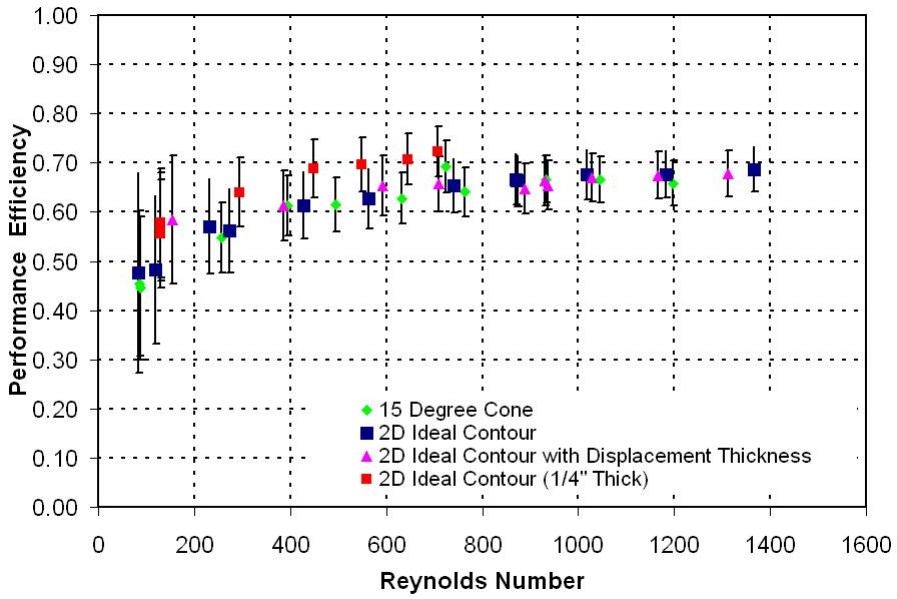

Figure 4-11: Performance Efficiency versus Reynolds Number for Nozzles with 100% Axial Lengths. Error Bars are included.

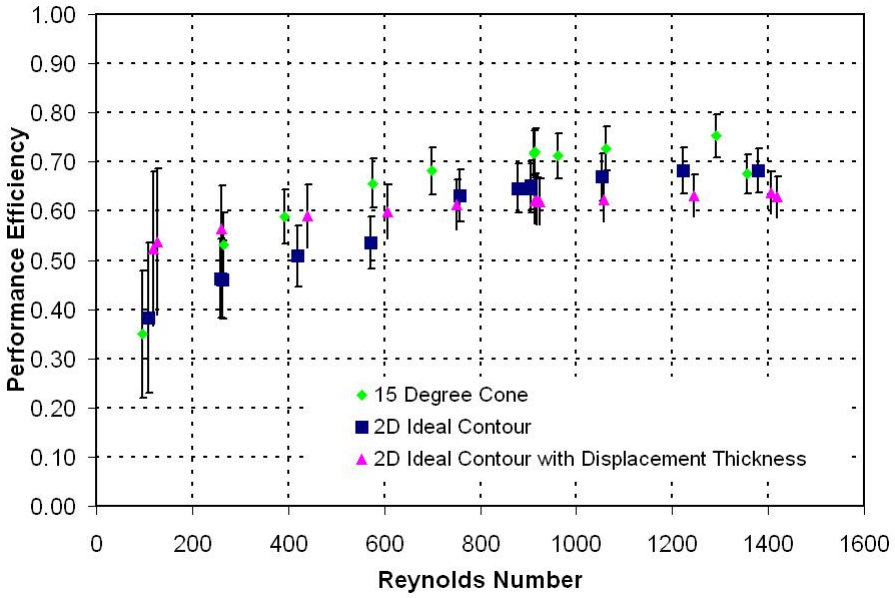

Figure 4-12: Performance Efficiency versus Reynolds Number for Nozzles with 50% Axial Lengths. Error Bars are included.

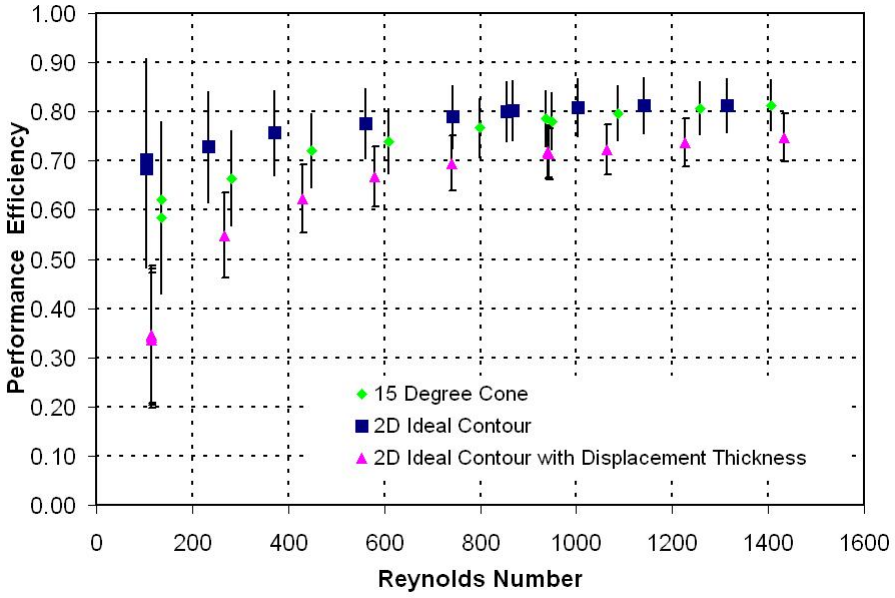

Figure 4-13: Performance Efficiency versus Reynolds Number for Nozzles with 25% Axial Lengths. Error Bars are included.

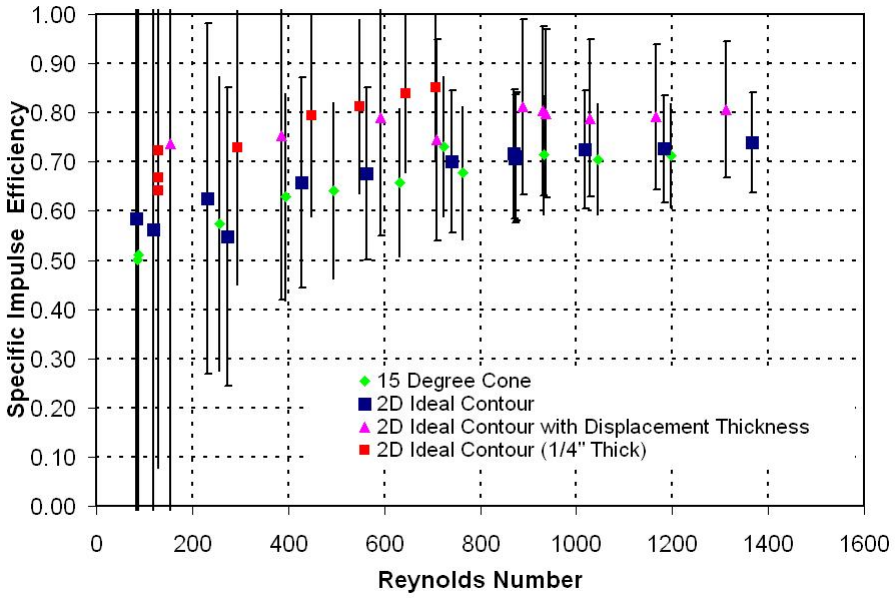

Figure 4-14: I_{sp} Efficiency versus Reynolds Number for Nozzles with 100% Axial Lengths. Error Bars are included.

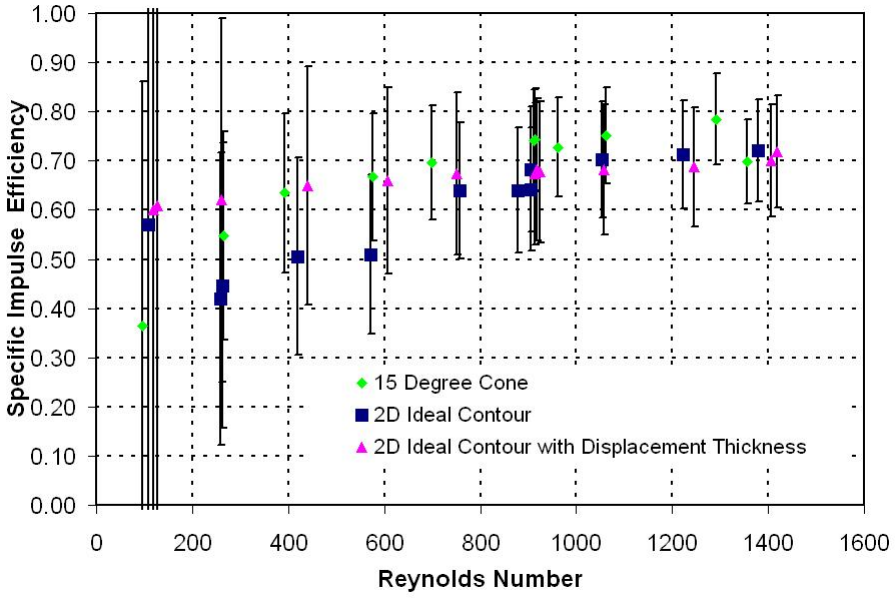

Figure 4-15: I_{sp} Efficiency versus Reynolds Number for Nozzles with 50% Axial Lengths. Error Bars are included.

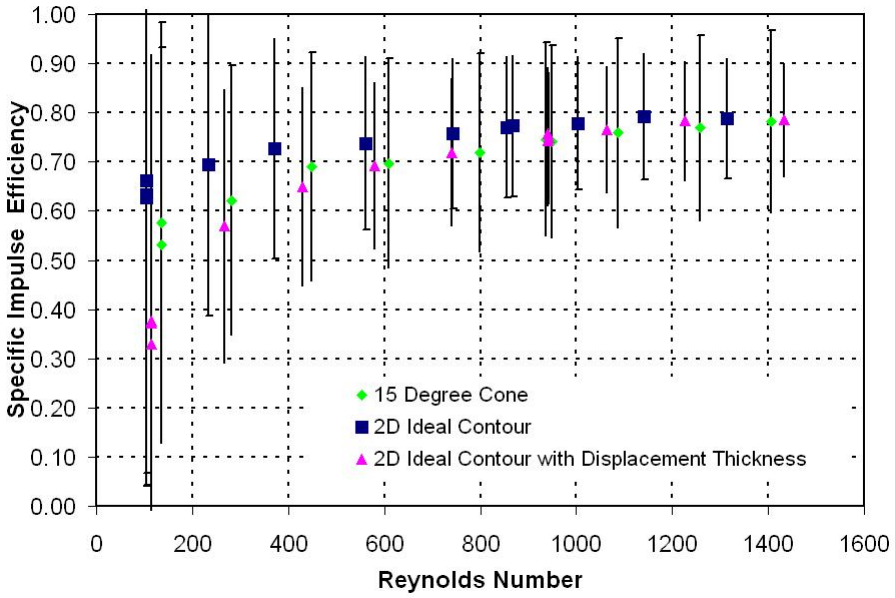

Figure 4-16: I_{sp} Efficiency versus Reynolds Number for Nozzles with 25% Axial Lengths. Error Bars are included.

The I_{sp} efficiency results are consistent with the thrust efficiency. There is a noticeable improvement (5%) with the reduction in axial lengths of the nozzles. This makes sense since the back pressure effects act on the nozzle exit cross section, which is reduced with shorter nozzles. The I_{sp} efficiency results are more closely related to the thrust efficiency since the back pressure is accounted for. Furthermore the performance efficiency is in excess of 70% for 100% expansion and 80% for 25% expansion for Reynolds numbers above a 1,000. This is very good, and further suggest acceptable efficiency can be obtained from low Reynolds numbers nozzles. The mass flow rate is calculated assuming isentropic flow, which means the actual mass flow is lower and hence the efficiency is likely higher than plotted here. With this generous assumptions the efficiency is in excess of 80% for Reynolds numbers above 600. This goes beyond the experimental requirement of demonstrating 80% thrust efficiency by demonstrating high I_{sp} as well.

4.4 Error Analysis

The error analysis is done by summing influence of multiple uncertainties as they propagate through the functions of interests. The first order error analysis is done by taking the partial derivative with respect to each variable that has uncertainty and then multiplying that by the uncertainty. The absolute value is then taken and this is repeated for all variables with uncertainty and summed together to generate the net error. Formally this is;

$$\Delta F = \sum_{i=1}^{N} |\frac{\partial F}{\partial x_i} \Delta x_i|, \tag{4.16}$$

where F is the function of interests, x_i are the independent variables and Δx_i are the known uncertainties. Below is a table with the known experimental uncertainties.

Variable	Error
Throat Area (A_*)	8.065^{-8} m^2
Exit Area (A_e)	8.065^{-8} m^2
Ambient Pressure (P_a)	500 Pascals
Chamber Pressure (P_0)	500 Pascals
Thrust (T)	.0014 Newtons
Mach Number (M)	.25 (.70 for the 25% 15 Degree Cone)

Table 4.1: Summary of Significant Uncertainties

The area errors are from the measurement and manufacturing uncertainty in the machine shop. The pressure and thrust error are from the transducer and thrust stand uncertainty. The Mach number error is calculated by perturbing the nozzle geometries and numerically finding the corresponding changes in Mach number. The error analysis is tedious, and one example calculation is outlined here for finding the corrected I_{sp} efficiency. The corrected I_{sp} efficiency is defined simply as the measured result divided by the theoretical maximum;

$$\eta_{I_{sp}Corrected} = \frac{I_{sp}Corrected}{I_{sp}Isentropic} = \frac{u_eCorrected}{u_eIsentropic}. \tag{4.17}$$

Since I_{sp} is exhaust velocity divided by g_0, the constant is removed and the analysis is done in terms of exhaust velocity efficiency. The uncertainty in the efficiency is then found by applying equation 4.16;

$$\Delta\eta_{I_{sp}Corrected} = \frac{1}{u_e Isentropic}\Delta u_e Corrected + \frac{u_e Corrected}{u_e Isentropic^2}\Delta u_e Isentropic. \quad (4.18)$$

The measured exhaust velocity is calculated by multiply equation 4.12 by g_0,

$$u_e Corrected = \frac{T - (P_e - P_a)A_e}{\dot{m}}. \quad (4.19)$$

As stated previously, the exit pressure and mass flow rate are calculated with isentropic relations since equipment is not available to directly measure them. As a result the errors are assumed from uncertainties in the known quantities used to calculate them in the context of the isentropic assumptions. In order to make this more tractable, the $\Delta u_e Corrected$ needs to be broken down and a new expression for $\dot{m}$ can be found in term of the chamber pressure, temperature and throat area;

$$\dot{m} = \rho A_* V = (\frac{2}{\gamma+1})^{\frac{1}{\gamma-1}}\frac{P_0}{RT_0}A_*\sqrt{\gamma R\frac{2}{\gamma+1}T_0} = (\frac{2}{\gamma+1})^{\frac{1}{\gamma-1}}\sqrt{\gamma\frac{2}{\gamma+1}}\frac{P_0}{\sqrt{RT_0}}A_*. \quad (4.20)$$

$u_e Corrected$ can now be written as;

$$u_e Corrected = C_1\frac{\sqrt{RT_0}}{P_0 A_*}(T - (P_e - P_a)A_e), \quad (4.21)$$

where C_1 is a function of γ from equation 4.20. The uncertainty in $u_e Corrected$ is now;

$$\begin{aligned}\Delta u_e Corrected \;=\; & C_1\sqrt{RT_0}\left(\frac{1}{P_0 A_*}\Delta T + \frac{T}{{P_0}^2 A_*}\Delta P_0 + \frac{T}{A_*^2 P_0}\Delta A_* + \right.\\ & \frac{(P_e - P_a)}{P_0 A_*}\Delta A_e + \frac{(P_e - P_a)A_e}{A_*^2 P_0}\Delta A_* + \frac{(P_e - P_a)A_e}{{P_0}^2 A_*}\Delta P_0 + \\ & \left.\frac{A_e}{P_0 A_*}\Delta P_e + \frac{A_e}{P_0 A_*}\Delta P_a\right)\end{aligned} \quad (4.22)$$

The uncertainty in ΔP_e can be found from the uncertainty in Mach number and P_0, starting with;

$$P_e = P_0 \left(1 + (\frac{\gamma - 1}{2})M^2\right)^{\frac{-\gamma}{\gamma-1}}, \tag{4.23}$$

and taking the partial derivatives with respect to Mach number and P_0 yields,

$$\Delta P_e = \left(1 + (\frac{\gamma - 1}{2})M^2\right)^{\frac{-\gamma}{\gamma-1}} \Delta P_0 + P_0 \frac{-\gamma}{\gamma - 1} \left(1 + (\frac{\gamma - 1}{2})M^2\right)^{(\frac{-\gamma}{\gamma-1}-1)} 2(\frac{\gamma - 1}{2})M\Delta M. \tag{4.24}$$

This expression can substituted into equation 4.22 to find the $\Delta I_{sp}Corrected$. An expression for $\Delta u_e Isentropic$ can be found by taking the derivative of the isentropic exhaust velocity with respect to $\frac{P_e}{P_0}$. The ideal case is the isentropic exhaust velocity calculated by conserving enthalpy;

$$u_e = \sqrt{\frac{2\gamma RT_0}{(\gamma - 1)\bar{M}} \left(1 - \left(\frac{P_e}{P_0}\right)^{\frac{(\gamma-1)}{\gamma}}\right)}. \tag{4.25}$$

The uncertainty is;

$$\Delta u_e Isentropic = \sqrt{\frac{2\gamma RT_0}{(\gamma - 1)\bar{M}}} \frac{1}{2} \left(1 - \left(\frac{P_e}{P_0}\right)^{\frac{\gamma-1}{\gamma}}\right)^{-\frac{1}{2}} \frac{\gamma - 1}{\gamma} \left(\frac{P_e}{P_0}\right)^{(\frac{\gamma-1}{\gamma}-1)} \Delta\frac{P_e}{P_0}, \tag{4.26}$$

where $\Delta\frac{P_e}{P_0}$ is,

$$\Delta\frac{P_e}{P_0} = \frac{-\gamma}{\gamma - 1} \left(1 + (\frac{\gamma - 1}{2})M^2\right)^{(\frac{-\gamma}{\gamma-1}-1)} 2(\frac{\gamma - 1}{2})M\Delta M. \tag{4.27}$$

$\Delta u_e Isentropic$ is substituted into equation 4.18 to find the uncertainty in the overall $\eta_{I_{sp}Corrected}$. This is a very tedious process and it is calculated in Microsoft Excel. The uncertainty in this experiment is quite large and both the thrust and I_{sp} efficiency uncertainty grows at lower Reynolds numbers. This is a result of the pressure transducer's limited accuracy at lower pressures. At Reynolds numbers above 1,000 the uncertainty is below 10%, which is acceptable. Furthermore even though the error bars are quite large (50%), there is consistency in the results which allows for

qualitative conclusions to be drawn.

Chapter 5

Elementary Analysis on the System and Conclusions

5.1 Systems Analysis

The simplest chemical space propulsion thruster consists of the propellant tank, pressurant gas, propellant lines, valves, power for the valves, a catalyst bed for the propellant and a nozzle. The single tank configuration allows for the simplest system; however, the pressure of the propellant will decrease as the tank blows down. For a single tank where the initial fuel volume fraction is 40%, the initial pressure needs to be roughly 2.33 times the final pressure as per equation 1.12. This will change the thrust during the lifetime of the thruster which may be acceptable for many missions where a factor of two in thrust variation is negligible.

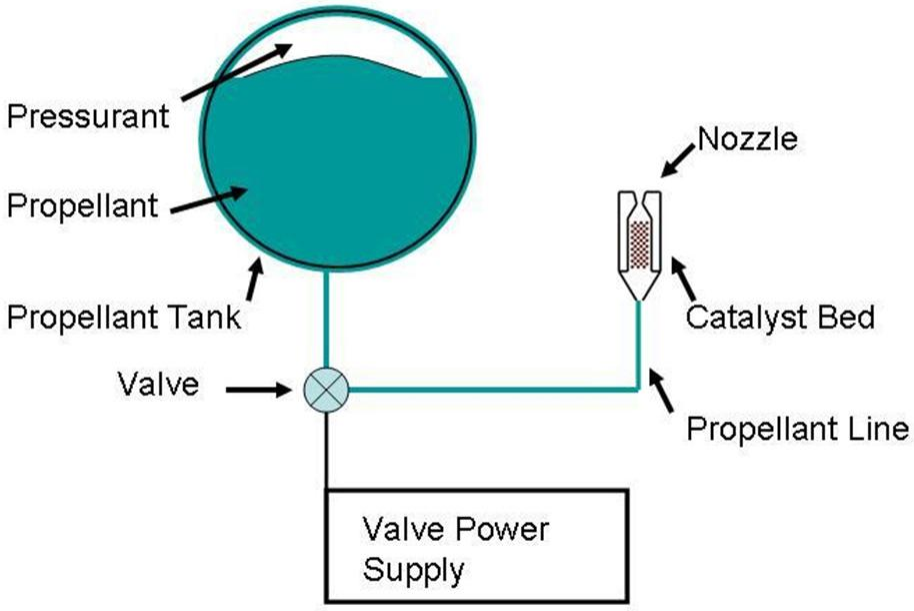

Figure 5-1: System level view of elementary thruster with a single tank configuration

The tank mass for a 200 m/s ΔV mission is approximately 1 kg for peroxide propellant with an I_{sp} is 127 seconds from figure 1-1, and the diameter is 13 cm from figure 1-3. Hydrogen peroxide is used in this example since it is the desired propellant for the design because it is environmentally friendly. Hydrazine is a better propellant since it is more storable and has a higher I_{sp}. The valve to control the flow is a technical challenge that has received a lot of attention recently due to improvement in micro fabrication technology. The two most popular designs use either electrostatic or reverse piezoelectric forces to operate the valve. The reverse piezoelectric effect is to generate a strain and stress by applying a voltage across a crystal. Piezoelectric technology is promising since pressures on the order of 10 MPa can be generated. For example with a typical material such as lead zirconate titanate (PZT) a strain of 0.001 can generated and the Young's modulus is approximately 63 GPa, that yields a stress of 63 MPa [5]. Piezoelectric valve technology for space technology was advanced largely be efforts at the Jet Propulsion Laboratory. For example, a piezoelectric valve was built and tested at inlet pressures of 35 psi [5]. Piezoelectric

valve technology looks appealing for future efforts; however, it is not considered for this project for two reasons: It is immature and fabrication techniques are still in development to properly address the high pressures. Secondly, piezoelectric materials have a low Curie temperature (the maximum temperature for piezoelectricity), for example PZT becomes inactive at 350 degrees C [38]. This prevents the valves from being mounted near the thruster which in past efforts was a serious problem since the valves would ideally be mounted on the same silicon chip as the thruster [16]. Furthermore the design team from Ventions had experience with electrostatic valves and wanted analysis for that technology.

As a result, the electrostatic design is briefly evaluated for this design and it involves applying a voltage across two plates to generate a force. The concept was looked at back when there was an active microengine program at the MIT Gas Turbine Lab. The concept is limited by the electric field strength;

$$p = \frac{1}{2}\epsilon_0 E^2, \tag{5.1}$$

where ϵ_0 is the permittivity of free space and E is the electric field between the plates. Electric field breakdown effects limit the voltage across the plates as well as the spacing [47]. Practically with 300 volts and 4 μm of spacing yields approximately .25 atm of pressure. This is quite small and means that a valve acting against 30 atm of fluid pressure must have an area ratio of 120:1. The design is simple and the valve will still be no bigger than a cm on a side.

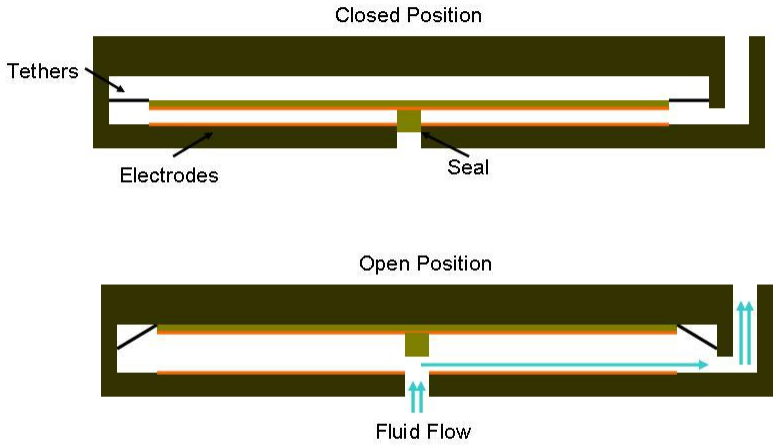

Figure 5-2: Elementary Electrostatic Valve Concept

In the concept depicted in 5-2, a voltage is applied between the electrodes to either hold the seal in place or push the plates apart to allow the fluid to flow. Tethers are depicted to hold the moving plate and they get stretched as the plate moves. A similar valve for operating a microengine in atmospheric conditions was designed, built and tested at MIT by Yang [48] in 2001. The valve operated against 10 atm of pressure, had a maximum flow rate of 3.38 g/hr, consumed less than 0.04 mW of power and was 1.64 mm on a side. The power requirements will be similar for this valve and the mass for batteries and solar panels for this item alone will easily be under 30 grams [13]. The other two components are the catalyst bed and the feedlines. The Catalyst bed can be made from a number of catalyst and silver is a common choice for Peroxide. The bed will be on the order of the size of the nozzle exit and this should not present too many difficulties since the ratio of surface area to volume increases on the micro scale. The feedlines will be in a Poiseuille flow regime and follow;

$$\Delta p = \frac{8\mu Q L}{\pi r^4}, \tag{5.2}$$

where μ is the dynamic viscosity, Q is the volumetric flow rate and L is the length. If the lines more than 50 μm in diameter and less than 20 cm long, than the pressure losses in the lines should be less than 10 atm using equation 5.2. The dominant mass and volume component for this design is the propellant tank which is approximately 1 kg. The other components will not be a significant mass or volume of the spacecraft (less than 1%).

5.2 Conclusion

It has been demonstrated that a nozzle with a Reynolds number of 650 or above can operate at greater than 80% thrust efficiency. The other system level components will be of negligible mass and such a thruster will have a factor of two improvement over cold gas butane thrusters. Electric propulsion presents clear advantages in fuel savings with $I_{sp}s$ in excess of a 1,000 seconds. However for a 5 kg satellite, a 10 mN thruster requires at least 100 watts of power assuming it is 50% efficient. The power supply alone outweighs the satellite assuming it has a specific mass of 50g/W [26]. A chemical propulsion system is currently the best option for a satellite on the order of 5 kg where thrust in excess of 10 mN is required. The mass of current Hall thrusters capable of 10 mN is on the order of a kg without fuel or power. There is however research in ionic liquid electrospray thruster arrays that could bring the mass of a thruster well below a kg [20]. These thrusters draw a steady beam of ionized liquid with a voltage applied across two plates. Each emitter of mass provides on the order μN of thrust and the current research is packing multiple emitters into arrays to generate higher thrusts. A lightweight high thrust electric propulsion system coupled with a low mass power supply is required to replace the 10 mN chemical thruster described here.

5.3 Future Work

The nozzle experiments demonstrated greater than 80% thrust efficiency and is considered a success though the error bars are quite large. Future experiments should be done with a more accurate pressure gauge which will eliminate most of the error. Furthermore a larger, or better pumped tank is preferable to keep the back pressure closer to the vacuum of space. This will eliminate much of the back pressure effects on the nozzle allowing for more accurate analysis of the I_{sp} efficiency. A mass flow controller should also be used to measure the mass flow directly as well. With better equipment or using MEMS technology, nozzles could be built closer to scale. A higher aspect ratio on the nozzles will also eliminate endwall boundary layer effects which will allow for a more accurate comparison between various contours. It would also be useful to test a sharp faced orifice and a nozzle with no expansion region downstream of the throat to directly observe improvements with the nozzles. It is possible; however, unlikely that viscous effects in the subsonic region are responsible for the majority of the inefficiency. The flow is accelerating strongly there which reduced viscous effects; however, that possibility can not be eliminated. These nozzles are operating at Knudsen numbers above .01 according to figure 2-5, which is where the continuum assumption begins to break down ($(kn \sim 0.01 - 0.1)$ [44]. It is therefore possible that kinetic modeling may explain the inefficiencies observed where the continuum approximation is used and should be investigated further. Lastly a more detailed heat transfer analysis should be done to more precisely determine whether heat transfer from the nozzle wall contributes to the losses observed.

The overall system also needs development and testing. A high pressure, low power valve needs to be tested or alternatively a small pump needs to be developed. (Experiments with Electrokinetic pumps are underway by Patel et al. for small thrusters [2].) Preliminary designs are evaluated during this project for a valve, and that is a critical component for future efforts. Lastly a design for an actual thruster must account for heat transfer effects. There will be some losses as the nozzle and catalyst bed heat up to the reaction temperature; however, their thermal mass will be

low. It is imperative that the nozzle and catalyst bed are kept well thermally isolated from the rest of the spacecraft though. This could be done with tethers to keep the thermal resistance high.

At this stage clever engineering and good microfabrication techniques is what is required to build an efficient 10 mN chemical thruster. Many of the physical concerns have been addressed and a hardware development is now needed.

Appendix A

Nozzle Geometry Code

```
%Method of Characteristics
%Alexander Bruccoleri
%Isientropic Case Expansion

clear all

gam = 1.66; % Gamma
Mi = 1; % Initial Mach Number
Me = 4.8; % Final Mach Number
k = ((gam+1)/(gam-1)).^.5;
n = 20; % Number of Mach Lines
m = (n^2+n)/2;
wmin = 180/pi*(k*atan((((Mi.^2)-1).^.5)/k)-atan(((Mi.^2)-1).^.5));
%Prandtl-Meyer Function Min
wmax = 180/pi*(k*atan((((Me.^2)-1).^.5)/k)-atan(((Me.^2)-1).^.5));
%Prandtl-Meyer Function Max
vmax = wmax*.5*pi*(1/180);
invariancep(1,1) = wmax; % Maximum Positive Invariant
invariancen(1,1) = -wmin; % Minimum Positive Invariant

dInv = (wmax-wmin)/(n-1); % Assume Uniform Change in Invariant
```

```
% First Loop Solves for Positive and Negative Invariants at all
% Intersections of Mach Waves
for i = 2:n
    for j = 1:i
        invariancep(i,j) = invariancep(i-1,1)+(-2+j)*ΔInv;
        invariancen(i,j) = invariancen(1,1)-(-1+j)*ΔInv;
    end
end

theta(:,:) =  (invariancep(:,:)+invariancen(:,:))/2;
%Solve for Theta
w(:,:) = invariancep(:,:)-theta(:,:);
%Solve for Prandlt Meyer Function

M = [0:.01:(Me+.1)]; % Creat an Array of possible Mach numbers

%Solve for the Mach Number at each wave intersection
for i = 1:n
    for j = 1:i
        func(i,j,:) = abs(-w(i,j)+180/pi*(k*atan...
            ((((M.^2)-1).^.5)/k)-atan(((M.^2)-1).^.5)));
        [C,s(i,j)] = min(func(i,j,:));
        Mach(i,j) = M(s(i,j));
    end
end

u1(:,:) = (180/pi)*real(asin(1./Mach(:,:))); % Mach Angle
u(:,:) = (pi/180)*cat(2,u1(:,1)-wmax/2,u1(:,[2:n]));
% Adjusted Mach Angle
%Except at first symmetry line
u(n,1) = (pi/180)*u1(n,1);
ur(:,:) = (pi/180)*u1(:,:); % Mach Angle in Radians
b1(:,:) = (pi/180)*(theta(:,:)+u1(:,:)); % Angle b
a1(:,:) = (pi/180)*(-theta(:,:)+u1(:,:)); % Angle a
```

```
%These loops average the angles a and b.
for i = 1:n
    for j = 1:i
        if i == j
            b(i,j) = b1(i,j);
        else
            b(i,j) = .5*(b1(i,j)+b1(i-1,j));
        end
        if i == n || j == n
            a(i,j) = b1(i,j);
        else
            a(i,j) = .5*(a1(i,j)+a1(i+1,j+1));
        end

    end
end

%This loop solces for the position of the mach wave interections

for i = 1:n
    for j = n:-1:i
        % Along the first column of intersections the calaculations
        %  are easier since the mach angle is know from the corner
        %  at point, (0,1).
        if i == 1
            %The first reflection is trivial to solve since it is on
            %the y=0 axis.
            if j == n
                L(j,i)=(((1/tan(ur(n,1)))^2)+1)^.5;
                xp(j,i) = cos(ur(j,i))*L(j,i);
                yp(j,i) = 0;
            else
                %The other interections require using the
                %law of sines in the simple region.
                L(j,i) = (sin(pi-u(j+1,i)-b(j+1,i))./...
```

```
            sin(b(j+1,i)+u(j,i))).*L(j+1,i);
        xp(j,i) = cos(u(j,i))*L(j,i);
        yp(j,i) = 1-sin(u(j,i))*L(j,i);
        N(j+1,i) = (((xp(j,i)-xp(j+1,i)).^2)+...
            ((yp(j,i)-yp(j+1,i))...
            .^2)).^.5;
    end
end
%This if statement accounts for the non simple region.
% Please see attached diagram for trignometry definitions.
% Note, the numbering is different than the diagrams and
% they are there to be a guide for anyone interested in
% recreating and/or improving this code.
if i>1
    %This finds the positions of the reflections on the axis y =
    %0. See drawings for trignometry.
    if j == n
        L(j,i) = (sin(b(j,i-1))./sin(a(j-1,i-1)))*N(j,i-1);
        xp(j,i) = xp(j-1,i-1)+cos(a(j-1,i-1))*L(j,i);
        yp(j,i) = yp(j-1,i-1)-sin(a(j-1,i-1))*L(j,i);

        if ((yp(j-2,i-1)-yp(j,i)))>0 && ((xp(j-2,i-1)-xp(j,i)))>0

            G(j,i) = abs(atan(((yp(j-2,i-1)-yp(j,i))./((xp(j-2,...
                i-1)-xp(j,i)))));

        else

            G(j,i) = pi-abs(atan(((yp(j-2,i-1)-yp(j,i))./...
                ((xp(j-2,i-1)-xp(j,i)))));

        end

        H(j,i) = pi-G(j,i);
        if G(j,i)>b(j,i)
            T(j,i) = G(j,i)-b(j,i);
```

```
        V(j,i) = H(j,i)-a(j-2,i-1);
    else
        T(j,i) = b(j,i)-G(j,i);
        V(j,i) = 2*pi-(H(j,i)-a(j-2,i-1));
    end
    V(j,i) = H(j,i)-a(j-2,i-1);
    w1(j,i) = pi-V(j,i)-T(j,i);
    Z(j,i) = (((yp(j-2,i-1)-yp(j,i)).^2)+((xp(j-2,i-1)-...
        xp(j,i)).^2)).^.5;
    N(j,i) = (sin(V(j,i))./sin(w1(j,i))).*Z(j,i);
    L(j-1,i) = (sin(T(j,i))./sin(w1(j,i))).*Z(j,i);
    xp(j-1,i) = xp(j-2,i-1)+cos(a(j-2,i-1))*L(j-1,i);
    yp(j-1,i) = yp(j-2,i-1)-sin(a(j-2,i-1))*L(j-1,i);
end
%This finds the intersection of the mach waves in the non
%simple regions.
if j>i
    % Quadrant 1 on unit circle.
    if ((yp(j-2,i-1)-yp(j,i)))>0 && ...
            ((xp(j-2,i-1)-xp(j,i)))>0

        G(j,i) = abs(atan(((yp(j-2,i-1)-yp(j,i))./...
            ((xp(j-2,i-1)-xp(j,i)))));

        H(j,i) = pi-G(j,i);
        if G(j,i)>b(j,i)
            T(j,i) = G(j,i)-b(j,i);
            V(j,i) = H(j,i)-a(j-2,i-1);
        else
            T(j,i) = b(j,i)-G(j,i);
            V(j,i) = 2*pi-(H(j,i)-a(j-2,i-1));
        end

        w1(j,i) = pi-V(j,i)-T(j,i);
        Z(j,i) = (((yp(j-2,i-1)-yp(j,i)).^2)+...
            ((xp(j-2,i-1)-xp(j,i)).^2)).^.5;
```

```
    N(j,i) = (sin(V(j,i))./sin(w1(j,i))).*Z(j,i);
    L(j-1,i) = (sin(T(j,i))./sin(w1(j,i))).*Z(j,i);
    xp(j-1,i) = xp(j-2,i-1)+cos(a(j-2,i-1))*L(j-1,i);
    yp(j-1,i) = yp(j-2,i-1)-sin(a(j-2,i-1))*L(j-1,i);
    % Quadrant 2 on unit circle.
elseif ((yp(j-2,i-1)-yp(j,i)))>0 && ...
        ((xp(j-2,i-1)-xp(j,i)))<0

    G(j,i) = pi-abs(atan(((yp(j-2,i-1)-yp(j,i))./...
        ((xp(j-2,i-1)-xp(j,i)))));

    H(j,i) = pi-G(j,i);
    if G(j,i)>b(j,i)
        T(j,i) = G(j,i)-b(j,i);
        V(j,i) = H(j,i)-a(j-2,i-1);
    else
        T(j,i) = b(j,i)-G(j,i);
        V(j,i) = 2*pi-(H(j,i)-a(j-2,i-1));
    end

    w1(j,i) = pi-V(j,i)-T(j,i);
    Z(j,i) = (((yp(j-2,i-1)-yp(j,i)).^2)+...
        ((xp(j-2,i-1)-xp(j,i)).^2)).^.5;
    N(j,i) = (sin(V(j,i))./sin(w1(j,i))).*Z(j,i);
    L(j-1,i) = (sin(T(j,i))./sin(w1(j,i))).*Z(j,i);
    xp(j-1,i) = xp(j-2,i-1)+cos(a(j-2,i-1))*L(j-1,i);
    yp(j-1,i) = yp(j-2,i-1)-sin(a(j-2,i-1))*L(j-1,i);

else
    % Quadrant 3 on unit circle.


    G(j,i) = abs(atan(((yp(j-2,i-1)-yp(j,i))./((xp(j-2,...
        i-1)-xp(j,i)))));
    H(j,i) = pi-G(j,i);
    T(j,i) = abs(a(j-2,i-1))-abs(G(j,i));
```

```
                    V(j,i) = 2*pi-(H(j,i)+b(j,i)); % Change to plus beta


                    w1(j,i) = pi-V(j,i)-T(j,i);
                    Z(j,i) = (((yp(j-2,i-1)-yp(j,i)).^2)+((xp(j-2,i-1)-...
                        xp(j,i)).^2)).^.5;
                    N(j,i) = (sin(V(j,i))./sin(w1(j,i))).*Z(j,i);
                    L(j-1,i) = (sin(T(j,i))./sin(w1(j,i))).*Z(j,i);
                    xp(j-1,i) = xp(j,i)+cos(b(j,i))*L(j-1,i);
                    yp(j-1,i) = yp(j,i)+sin(b(j,i))*L(j-1,i);

                end

            end

        end
    end
end

%Finds Theta at the corner in radians.
thetar1(1) = vmax;

%Finds theta for each point in the simple region.
%See attached diagram for trignometry definitions. Note, the
%numbering is different than the diagrams and they are there to be
%a guide for anyone interested in recreating and/or improving this
%code.
for i = 2:n+1
    thetar1(i) = (pi/180)*theta(i-1,i-1);
    thetar(i-1) = .5*(thetar1(i-1)+thetar1(i));
    %Average theta at wall.
end

%This loop find the position of the points along the nozzle wall.
tf = 0;
for i = 1:n
```

```
%Solves for the first point after the throat
if i == 1
    Lw(i) = ((xp(i,i)-0).^2+(yp(i,i)-1).^2).^.5;
    Wall(i) = (sin(ur(i,i))./(sin(b(i,i)-thetar(i))))*Lw(i);
    xpWall(i) = xp(i,i) + cos(b(i,i))*Wall(i);
    ypWall(i) = yp(i,i) + sin(b(i,i))*Wall(i);
else

    Lw(i) = ((xpWall(i-1)-xp(i,i)).^2+(ypWall(i-1)-...
        yp(i,i)).^2).^.5;
    % Quadrant 1 on unit circle.
    if ((ypWall(i-1)-yp(i,i)))>0 && ((xpWall(i-1)-xp(i,i)))>0
        tf(i) = 1;
        Gw(i) = abs(atan(((ypWall(i-1)-yp(i,i))./((xpWall...
            (i-1)-xp(i,i)))));
        Wall(i) = Lw(i).*(sin(abs(Gw(i)-b(i,i))./sin(b(i,i)...
            -thetar(i)));
        xpWall(i) = xpWall(i-1) + cos(thetar(i))*Wall(i);
        ypWall(i) = ypWall(i-1) + sin(thetar(i))*Wall(i);
        % Quadrant 2 on unit circle.
    elseif ((ypWall(i-1)-yp(i,i)))>0 && ((xpWall(i-1)-xp(i,i)))<0
        tf(i) = 2;
        Gw(i) = pi-abs(atan(((ypWall(i-1)-yp(i,i))./...
            ((xpWall(i-1)-xp(i,i)))));
        Wall(i) = Lw(i).*(sin(pi-Gw(i)+thetar(i))./...
            sin(b(i,i)-thetar(i)));
        xpWall(i) = xp(i,i) + cos(b(i,i))*Wall(i);
        ypWall(i) = yp(i,i) + sin(b(i,i))*Wall(i);
        % Quadrant 3 on unit circle.
    elseif ((ypWall(i-1)-yp(i,i)))<0 && ((xpWall(i-1)-xp(i,i)))<0
        tf(i) = 3;
        Gw(i) = abs(atan(((ypWall(i-1)-yp(i,i))./((xpWall(i-1)...
            -xp(i,i)))));
        Wall(i) = Lw(i).*(sin(abs(-Gw(i)+thetar(i))./sin(b(i,i)...
            -thetar(i)));
        xpWall(i) = xp(i,i) + cos(b(i,i))*Wall(i);
```

```
            ypWall(i) = yp(i,i) + sin(b(i,i))*Wall(i);
        end

    end
end

%Plot the points
for i = 1:n
    for j = 1:i
        Mach1(i) = Mach(i,i);

    end
end


figure(1)
plot(xp,yp,'+','MarkerSize',16)
hold on
%figure(2)
%plot(xpWall,ypWall)
```

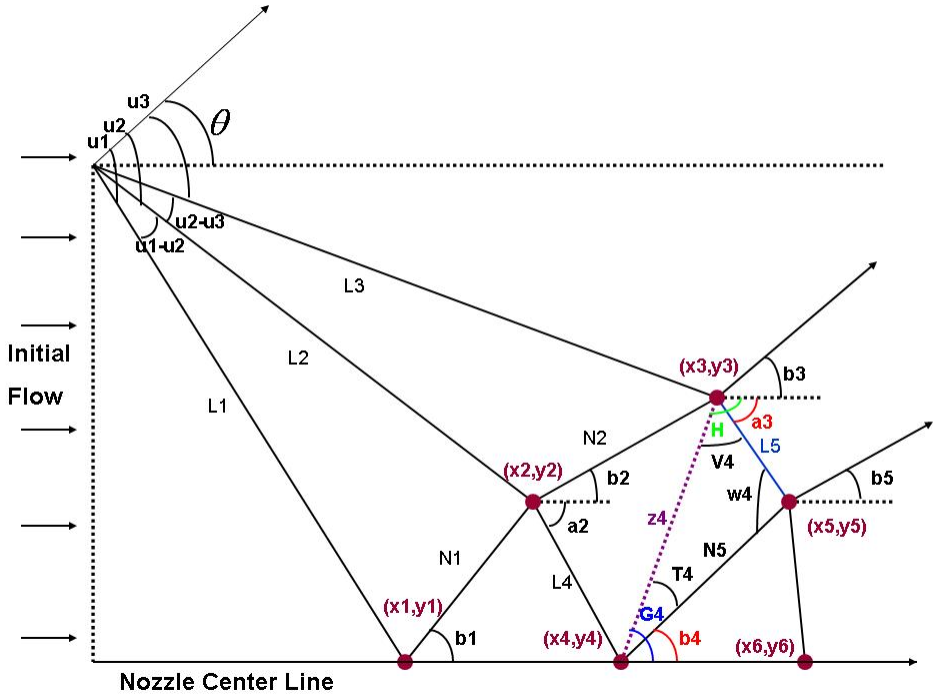

Figure A-1: Mach Wave Intersection in Nonsimple Region to Show Various Angles in the Code. (Only a few angles are labeled so the reader can identify them from the code.)

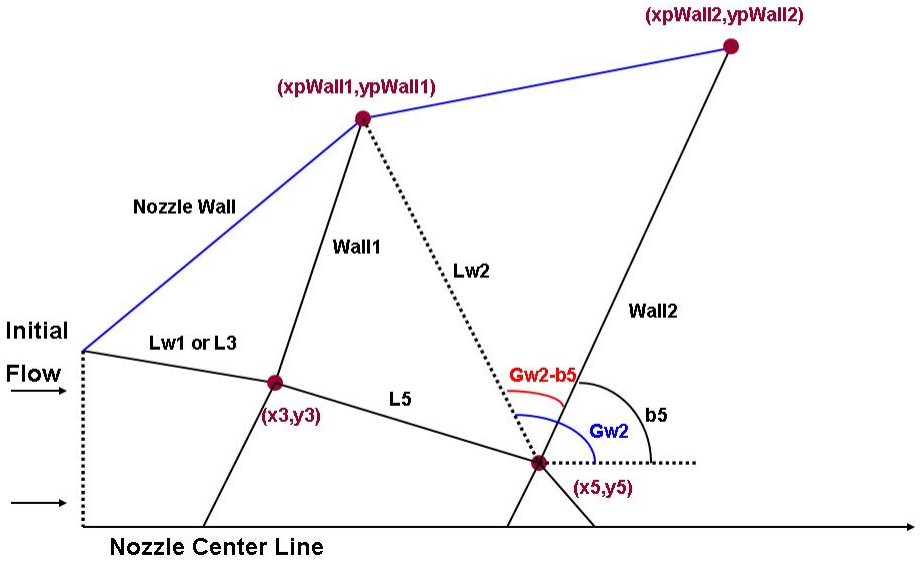

Figure A-2: Mach Wave Intersection near Wall Region to Show Various Angles in the Code. (This is an exaggerated figure for emphasis on how the angles are labeled.)

Also figure 2-6 is useful for understanding the code.

Appendix B

Influence Coefficient Code

```
%Alexander Bruccoleri
%Influence Coefficient Analysis

%This code lets the user assign an inlet mach number (Squared),
%  Stagnation Pressure and temperature.

%The user can have three independant variables change
% along the pipe, heat flow, friction and area change.

%  The code calculates the area, axial position, stagnation
%  pressure, static pressure, mach number squared and mach
%  number, temperature, Stagnation Temperature, Wall Temperature,
%  Reynolds and Knudsen number, and pressure ratio using the
%  influence coefficients.

% The code can start in subsomic flow and solve through
% supersonic. In this run, the code starts at the throat
% assuming sonic conditions.

% The user can then plot these results
```

```
n = 180; % number of steps, that you can play with
k = 4; % Second Loop iteration
L =.21E-3; % nozzle height
r = .9; % Recovery Factor
R = 775 % Gas Constant
mu = 3.37E-5; % Viscosity of the fluid

% Initialize Arrays
xposition = zeros(k,1);

%%%%%%%%%%Zero Mach^2, Temp, Stagnation Temp, Wall Temp,
% Pres., PresT, Nozzle Width, Velocity, Reynolds Number
% and Knudsen Number
M2 = zeros(k,n+1);
T = zeros(k,n+1);
Tt = zeros(k,n+1);
Twa = zeros(k,n+1);
P = zeros(k,n+1);
Pt = zeros(k,n+1);
w = zeros(k,n+1);
V = zeros(k,n+1);
Re = zeros(k,n+1);
Kn = zeros(k,n+1);
%%%%%%%%%%%%%%%%%%%%%%%%%%%%%%%%%%%%%%%%%%%%

%%%%%%%%%%%%%%%%%%%%%%%%%%%%%%%%%%%%%%%%%%%%These are
...the variables the user can play with!!!!
    gam = 1.37; % Gamma for air
M2(1:k,1) = 1.01; % Initial Mach Number SQUARED!
Tt(1:k,1) = 878; % Initial Total Temperature
Pt(1:k,1) = 1.2E6; % Initial Stagnation Temperature
w(1:k,1) = 35E-6; % Throat width

Q = 0;% 20000;% Heat Addition (h/(cp*mdot) assumimg cp & mdot are constant
%mdot is assumed 1E-4 kg/s
corse = .00001; % dx for low or high Mach numbers
```

```
fine = 5E-8; % dx for Mach numbers near 1
subangle = 3.14/6; % 30 degree Converging Section
superangle = 3.14/12; % 15 Degree Expansion Cone

T(1:k,1) = Tt(1:k,1)./(1+.5*(gam-1).*M2(1:k,1));
...% Initial Temperature
    P(1:k,1) = Pt(1:k,1)./((1+.5*(gam-1).*M2(1:k,1)).^ ...
    (gam/(gam-1))); % Initial Back Pressure
V(1:k,1) = (M2(1:k,1).^.5).*(gam*R*T(1:k,1)).^.5;
% Initial Velocity

%Initialize all variables to zero
%%%%%%%%%%%%%%%%%%%%%%%%
dx = zeros(k,n);
dr = zeros(k,n);
daA = zeros(k,n);


dM2Area = zeros(k,n);
dM2friction = zeros(k,n);
dM2heat = zeros(k,n);
dM2 = zeros(k,n);

dTHeat = zeros(k,n);
dTArea = zeros(k,n);
dTFriction = zeros(k,n);
dT =  zeros(k,n);

dTtHeat = zeros(k,n);
dTt =  zeros(k,n);

dPArea = zeros(k,n);
dPHeat = zeros(k,n);
dPFriction = zeros(k,n);
dP =  zeros(k,n);
```

```
dPtArea = zeros(k,n);
dPtHeat = zeros(k,n);
dPtFriction = zeros(k,n);
dPt =   zeros(k,n);

dVArea = zeros(k,n);
dVfriction = zeros(k,n);
dVheat = zeros(k,n);
dV = zeros(k,n);

M = zeros(k,n);
Aratio = zeros(k,n);
Pratio = zeros(k,n);
A(1:k,1) = L*w(1:k,1);
x = zeros(k,n+1);
f(1,1) = 0;
%%%%%%%%%%%%%%%%%%%%%%%%%%%%%%

for j = 1:4

    f(j) = 0.025*(j-1); %; % Frictional Coefficient


    for i = 1:n

        if M2(j,i) < .9
            dx(j,i) = corse; % If the Mach number
            % squared is low, step along x corsely.
            dw(j,i) = -2*tan(subangle)*dx(j,i);
            % Make the area smaller
            dQ(j,i) = Q*dx(j,i)*(2*(L+w(j,i)))*(Tt(j,i)-Twa(j,i));
            % Add Heat
```

```
elseif M2(j,i) ≥ .9 && M2(j,i) < 1
    dx(j,i) = fine; % If the Mach number is near one,
    % do a fine step.
    dw(j,i) = -2*tan(subangle)*dx(j,i);  % Make the
    % area smaller
    dQ(j,i) = Q*dx(j,i)*(2*(L+w(j,i)))*(Tt(j,i)-Twa(j,i));
    % Add Heat
elseif M2(j,i) ≥ 1 && M2(j,i) < 1.44
    dx(j,i) = fine; % If the Mach number is near one,
    % do a fine step.
    dw(j,i) = 2*tan(superangle)*dx(j,i); % Make the
    % area larger
    dQ(j,i) = Q*dx(j,i)*(2*(L+w(j,i)))*(Tt(j,i)-Twa(j,i));
    % Add Heat
else
    dx(j,i) = corse; % If the Mach number is large,
    % step along x corsely.
    dw(j,i) = 2*tan(superangle)*dx(j,i);
    % Make the area larger
    dQ(j,i) = Q*dx(j,i)*(2*(L+w(j,i)))*(Tt(j,i)-Twa(j,i));
    % Add Heat
end

w(j,i+1) = w(j,i)+dw(j,i); % Increment the width
A(j,i+1) = w(j,i+1)*L; % Increment the Area
x(j,i+1) = x(j,i)+dx(j,i); % Increment distance
daA(j,i) = (A(j,i+1)-A(j,i))/A(j,i); % Find Area Change
% normalized to Area

%%%%%%%%%%%Changes in Temperature
dTHeat(j,i) = (1./(Tt(j,i))).*dQ(j,i).*-((1+.5*(gam-1)* ...
    M2(j,i)).*(gam*M2(j,i)-1))./(1-M2(j,i)); % Influence
% of heat
dTArea(j,i) = (((gam-1).*M2(j,i))./(1-M2(j,i))).*T(j,i).*...
    daA(j,i);  % Influence of Area
```

```
dTFriction(j,i) = -((gam*(gam-1)*(M2(j,i).^2))./(2*(1-M2...
    (j,i)))).*(T(j,i)).*4*f(j)*dx(j,i).*(1/(2*L*w(j,i)/...
    (w(j,i)+L)));
%Influence of friction

dT(j,i) =  dTHeat(j,i)+dTFriction(j,i)+dTArea(j,i);
% Net change
%%%%%%%%%%%%%%%%%%%%%%%%%%%%%%%%%%%%%%%%%%%%%%%%%%

%%%%%%%%%%%%Changes in Total Temperature
dTtHeat(j,i) = dQ(j,i); % Influence of heat

dTt(j,i) =  dTHeat(j,i); % Net change
%%%%%%%%%%%%%%%%%%%%%%%%%%%%%%%%%%%%%%%%%%%%%%%%%%

%%%%%%% Changes in Pressure
dPArea(j,i) = (gam*M2(j,i)./(1-M2(j,i))).*daA(j,i).*P(j,i);
dPHeat(j,i) = ((-gam*M2(j,i).*(1+.5*(gam-1)*M2(j,i))./...
    (1-M2(j,i))).*P(j,i).*dQ(j,i)./(Tt(j,i));
dPFriction(j,i) = ((-gam*M2(j,i).*(1+(gam-1)*M2(j,i)))...
    ./(2*(1-M2(j,i)))).*P(j,i).*4*f(j)*dx(j,i).*(1/(2*L*...
    w(j,i)/(w(j,i)+L)));

dP(j,i) =   dPHeat(j,i)+dPFriction(j,i)+dPArea(j,i);
%%%%%%%%%%%%%%%%%%%%%%%%%%%%%%%%%%%%%%%%%%%%%%%%%%%%%%%%



%%%%%%% Changes in Total Pressure
dPtArea(j,i) = 0;
dPtHeat(j,i) = .5*(-gam*M2(j,i)).*Pt(j,i).*dQ(j,i)./...
    (Tt(j,i));
dPtFriction(j,i) = .5*(-gam*M2(j,i)).*P(j,i).*4*f(j)*...
    dx(j,i).*(1/(2*L*w(j,i)/(w(j,i)+L)));

dPt(j,i) =   dPtHeat(j,i)+dPtFriction(j,i)+dPtArea(j,i);
%%%%%%%%%%%%%%%%%%%%%%%%%%%%%%%%%%%%%%%%%%%%%%%%%%%%%%%%
```

```
%%%%%%%%%%%%%Changes in Mach Number
dM2Area(j,i) = ((((-2*(1+.5*(gam-1)*M2(j,i))).*(1-...
    M2(j,i))).*daA(j,i)).*(M2(j,i)));
dM2friction(j,i) = 4*f(j)*dx(j,i)*(1/(2*L*w(j,i)/(w(j,i)+...
    L)))*((((gam*M2(j,i)*(1+.5*(gam-1)*M2(j,i))).*...
    (1-M2(j,i)))).*(M2(j,i)));
dM2heat(j,i) = (dQ(j,i)*((gam*M2(j,i)+1).*(1+.5*(gam-1)...
    *M2(j,i)).*(1-M2(j,i))).*M2(j,i)).*(Tt(j,i));

dM2(j,i) = dM2heat(j,i)+dM2friction(j,i)+dM2Area(j,i);
%%%%%%%%%%%%%%%%%%%%%%%%%%%%%%%%%%%%%%%%%%%%%%%%

%%%%%%%%%%%%%Changes in Velocity
dVArea(j,i) = (-1./(1-M2(j,i))).*daA(j,i).*V(j,i);
dVfriction(j,i) = 4*f(j)*dx(j,i)*(1/(2*L*w(j,i)/(w(j,i)+L...
    )))*(((gam*M2(j,i))./(2*(1-M2(j,i)))).*(V(j,i)));
dVheat(j,i) = (dQ(j,i)*((1+.5*(gam-1)*M2(j,i)).*(1-M2(j,i)...
    )).*V(j,i)).*(Tt(j,i));

dV(j,i) = dVheat(j,i)+dVfriction(j,i)+dVArea(j,i);
%%%%%%%%%%%%%%%%%%%%%%%%%%%%%%%%%%%%%%%%%%%%%%%%

M2(j,i+1) = M2(j,i) +  dM2(j,i); % Iterate Mach Squared,
%temperature, pressure, total temperature and Velocity
T(j,i+1) = T(j,i)+ dT(j,i);
Tt(j,i+1) = Tt(j,i)+ dTt(j,i);
Twa(j,i+1) = T(j,i+1) + r*(Tt(j,i+1)-T(j,i+1));
P(j,i+1) = P(j,i) + dP(j,i);
Pt(j,i+1) = Pt(j,i) + dPt(j,i);
V(j,i+1) = V(j,i) + dV(j,i);
M(j,i) = M2(j,i)^.5; % Find Mach Number
den(j,i) = P(j,i)/(R*T(j,i)); % Density
Re(j,i) = (V(j,i)*den(j,i)*w(j,i))/mu; % Reynolds number
Kn(j,i) = ((.5*gam*3.1459).*M(j,i))./Re(j,i);
```

```
        % Knudsen Number

    end


    At(j,1) = min(A(j,:)); %Minimum Throat
    Aratio(j,:) = A(j,1:n)./At(j,1); % Area Ratio
    Pratio(j,:) = P(j,1:n)./Pt(j,1); % Pressure Ratio


    xmax(j) = max(x(j,:));
    xmaxmin = min(xmax);


end

%Plotting
for p = 1:k

    xposition(p,1) = min(find((xmaxmin-.00003) < x(p,:) & ...
        x(p,:) < (xmaxmin+.00003))-1);
    xnormal(p,:) = x(p,:)/xmaxmin;

    plot(xnormal(p,1:xposition(p,1)),Kn(p,1:xposition(p,1)))
    hold on

end
```

Bibliography

[1] John D. Anderson. *Modern Compressible Flow with Historical Perspective*, chapter 4,11, pages 85–118,260–305. McGraw-Hill Book Company, United States of America, 1982.

[2] Michael S. Bartsch, Matthew H. McCrink, Robert W. Crocker, Bruce P. Mosier, Kenneth A. Peterson, Karl Wally, and Kamlesh D. Patel. Electrokinetically pumped liquid propellant microthrusters for orbital station keeping. *The 14th International Conference on Solid-State Sensors, Actuators and Microsystems, Lyon France*, June 2007.

[3] Ferdinand P. Beer, Jr. E. Russell Johnston, and John T. DeWolf. *Mechanics of Materials 3rd EDITION*, chapter Appendix B., page 749. The McGraw-Hill Companies, Inc., New York, NY, 2001.

[4] G. Bird. *Molecular Gas Dynamics and the Direct Simulation of Gas Flows*, chapter 1.2. Clarendon Press, Oxford, England, UK, 1994.

[5] I. Chakraborty, W.C. Tang, D.P. Bame, and T.K. Tang. Mems micro-valve for space applications. *Sensors and Actuators A: Physical Journal*, 83:188–193, May 2000.

[6] IPS Corporation. Weld-On Acrylic Adhesives and Cements, Product Bulletin, 3, Acrylic Plastic Cement. Website, April 2009. `http://www.ipscorp.com/pdf/assembly/Assembly_PB3.pdf`.

[7] Omax Corporation. OMAX 2652 JetMachining Center. Website, April 2009. http://www.omax.com/machine.php?product=2652.

[8] Jr. David H. Lewis, Siegfried W. Jansony, Ronald B. Coheny, and Erik K. Antonsson. Digital micropropulsion. *12th IEEE International Micro Electro Mechanical Systems Conference (MEMS 99)*, January 1999.

[9] Mark Drela. Personal Communication, and direct assistance with solving a displacement thickness calculation, 2008.

[10] Omega Engineering. Solid State Pressure Transducer 0 to 5 Vdc or 4 to 20 mA Outputs Vacuum to 300 psi Ranges. Website, April 2009. http://www.omega.com/ppt/pptsc.asp?ref=PX209_PX219&Nav=preb04.

[11] N. Fitzgerald. Personal Communication between the authors of Internal Flow Concepts and Applications and Fitzgerald, 2002.

[12] Robert H. Frisbee. Advanced space propulsion for the 21st century. *Journal of Propulsion and Power Journal*, 19(6):1129–1154, November 2003.

[13] Mohit Garg, Marcus Franki, and Jennifer Sembera. Cubesat, Chapter 5.0, Power Subsytem. Website, April 2009. http://www.ae.utexas.edu/courses/ase463q/design_pages/spring03/cubesat/web/Paper%20Sections/5.0%20Power%20Subsystem.pdf.

[14] E. M. Greitzer, C. S. Tan, and M. B. Graf. *Internal Flow Concepts and Applications*, chapter 10, pages 513–515. Cambridge University Press, The Edinburgh Building, Cambridge, UK, 2006.

[15] Stanley P. Grisnik, Tamara A. Smith, and Larry E. Saltz. Experiment study of low reynolds number nozzles. *19th AIAA/DGLR/JSASS International Electric Propulsion Conference. AIAA-87-0992*, 1987.

[16] Jerry Guenette and Adam London. Personal communication with Jerry Guenette and Adam London of Ventions in the MIT GTL over the design of nozzles and valves, 2008.

[17] Philip G. Hill and Carl R. Peterson. *Mechanics and Thermodynamics of Propulsion 2nd ed.*, chapter 11, pages 513–559. Addison-Wesley Publishing Company, Inc, United States of America, 1992.

[18] Robert Hoyt, Jeffrey Slostad, and Robert Twiggs. The multi-application survivable tether (mast) experiment. *39th AIAA/ASME/SAE/ASEE Joint Propulsion Conference and Exhibit, Huntsville, Alabama*, 2003.

[19] Frank P. Incropera and David P. DeWitt. *Fundamentals of Heat and Mass Transfer 5th EDITION*, chapter Appendix A, Table A.4, page 919. John Wiley & Sons, Inc., United States of America, 2002.

[20] Robert S. Legge Jr. Fabrication and characterization of porous metal emitters for electrospray applications. Master of science in aeronautics and astronautics, Massachusetts Institute of Technology, June 2008.

[21] W Leiner K Altfield and M Fiebig. Second law optimization of flat plate solar air heaters. *Solar Energy*, 41:127–132, 1988.

[22] Andrew D. Ketsdever and Juergen Mueller. Systems considerations and design options for microspacecraft propulsion systems. *35th AIAA/ASMA/SAE/ASEE Joint Propulsion Conference and Exhibit. AIAA 99-2723*, June 1999.

[23] N. M. Kuluva and G. A. Hosack. Supersonic nozzle discharge at low reynolds numbers. *AIAA Journal*, 9(9):1876–1879, September 1971.

[24] Randy Leiter. Personal communication with Randy Leiter over the test stand operation, 2009.

[25] Adam Pollok London. *Development and Test of a Microfabricated Bipropellant Rocket Engine*. PhD dissertation, Massachusetts Institute of Technology, Department of Aeronautics and Astronautics, June 2000.

[26] Paulo Lozano. Personal communication with Paulo Lozano on spacecraft power supplies, 2009.

[27] M. Martinez-Sanchez and J. E. Pollard. Spacecraft electric propulsionan overview. *Journal of Propulsion and Power Journal*, 14(5):688–699, September 1998.

[28] Manuel Martinez-Sanchez. Lecture 3: Ideal nozzle fluid mechanics. Notes from MIT Course 16.512, Rocket Propulsion.

[29] Manuel Martinez-Sanchez. Lecture 4-5: Nozzle design: Method of characteristics. Notes from MIT Course 16.512, Rocket Propulsion.

[30] Manuel Martinez-Sanchez. Lecture 7: Heat transfer in rocket nozzles. Notes from MIT Course 16.512, Rocket Propulsion.

[31] Manuel Martinez-Sanchez. Personal communication with Manuel Martinez-Sanchez on friction and boundary layer scaling relations, 2009.

[32] P. F. Massier, L. H. Back, M. B. Noel, and F. Saheli. Viscous effects on the flow coefficient for a supersonic nozzle. *AIAA Journal*, 8(3):605–607, March 1970.

[33] Jareb Mirczak. Milli-newton thrust stand for electric propulsion. Master of science in aeronautics and astronautics, Massachusetts Institute of Technology, June 2003.

[34] Chris Morley. Gaseq, A Chemical Equilibrium Program for Windows. Website, May 2009. `http://www.gaseq.co.uk/`.

[35] Juergen Mueller, John Ziemer, Richard Hofer, Richard Wirz, and Timothy ODonnell. A survey of micro-thrust propulsion options for microspacecraft and formation flying missions. 5th Annual CubeSat Developers Workshop San Luis Obispo, CA, April 2008.

[36] Christopher S. Protz. *Experimental Investigation of Microfabricated Bipropellant Rocket Engines*. PhD dissertation, Massachusetts Institute of Technology, Department of Aeronautics and Astronautics, June 2004.

[37] Jr. Robert Louis Bayt. *Analysis, Fabrication and Testing of a MEMS-based Micropropulsion System*. PhD dissertation, Massachusetts Institute of Technology, Department of Aeronautics and Astronautics, May 1999.

[38] Ali Sayir and Alp Sehirlioglu. High-Temperature Piezoelectric Material Developed. Website, April 2009. `http://www.grc.nasa.gov/WWW/RT/2007/Str-Matl/10-RXC-sayir.html`.

[39] Ascher H. Shapiro. *The Dynamics and Thermodynamics of Compressible Fluid Flow*, volume 1, chapter 8, pages 219–260. John Wiley and Sons, United States of America, 1953.

[40] Michael D. Souder and Matthew West. The multi-application survivable tether (mast) experiment. *AIAA/AAS Astrodynamics Specialist Conference and Exhibit, Honolulu, Hawaii*, 2008.

[41] U.S. Department of the Treasury The United States Mint. About the united states mint, coin specifications. Website, April 2009. `http://www.usmint.gov/about_the_mint/?action=coin_specifications`.

[42] Philip A. Thompson. *Compressible-Fluid Dynamics*, chapter 9, pages 443–481. McGraw-Hill, United States of America, 1972.

[43] Varun and M K Mittal. Heat transfer and friction characteristics in rectangular channel having, inclined and transverse ribs on the absorber plate. *IE(I) Journal-MC*, 87:28, July 2006.

[44] D. L. Hitt W. F. Louisos. Supersonic micro-nozzles. This is a yet to be published article for the Dongquing Li: Encyclopedia of Micro- and Nano- Fluidics, Entry 230, 2008.

[45] Frank M. White. *Fluid Mechanics*, chapter 6, pages 366–376. McGraw-Hill, New York, NY 10020, 2003.

[46] Frank M. White. *Viscous Fluid Flow 3rd EDITION*, chapter 4, page 224. The McGraw-Hill Companies, Inc., New York, NY, 2006.

[47] Xue'en Yang. A mems valve for the mit microengine. Master of science in mechanical engineering, Massachusetts Institute of Technology, May 2001.

[48] Xue'en Yang, Alexander Hölke, Stuart A. Jacobson, Jeffrey H. Lang, Martin A. Schmidt, and Stephen D. Umans. An electrostatic, on/off microvalve designed for gas fuel delivery for the mit microengine. *Microelectromechanical Systems Journal*, 13(4):660–668, August 2004.